NEW YORK UNIVERSITY
INSTITUTE OF MATHEMATICAL SCIENCES
LIBRARY
25 Waverly Place, New York 3, N. Y.

AEC Computing Facility

NYO 7695

AEC RESEARCH AND DEVELOPMENT REPORT

PHYSICS NYO-7695

NON-LINEAR DEFLECTIONS OF SHALLOW SPHERICAL SHELLS*

by

Edward L. Reiss, Herbert J. Greenberg
and
Herbert B. Keller

December 31, 1956

institute of mathematical sciences

NEW YORK UNIVERSITY

NYO-7695
c.1

NEW YORK, NEW YORK

This report was prepared as an account of Government sponsored work. Neither the United States, nor the Commission, nor any person acting on behalf of the Commission:

A. Makes any warranty or representation, express or implied, with respect to the accuracy, completeness, or usefulness of the information contained in this report, or that the use of any information, apparatus, method, or process disclosed in this report may not infringe privately owned rights; or

B. Assumes any liabilities with respect to the use of, or for damages resulting from the use of any information, apparatus, method, or process disclosed in this report.

As used in the above, "person acting on behalf of the Commission" includes any employee or contractor of the Commission to the extent that such employee or contractor prepares, handles or distributes, or provides access to, any information pursuant to his employment or contract with the Commission.

AEC Computing Facility
Institute of Mathematical Sciences
New York University

PHYSICS NYO-7695

NON-LINEAR DEFLECTIONS OF SHALLOW SPHERICAL SHELLS*

by

Edward L. Reiss, Herbert J. Greenberg
and
Herbert B. Keller

December 31, 1956

---

*The research reported in this paper was performed under Contract AT(30-1)-1480 with the United States Atomic Energy Commission. A partial summary of the results contained in this paper was presented at the Ninth International Congress of Applied Mechanics in Brussels, Sept., 1956.

ABSTRACT

The equations obtained by Chien for the non-linear deflection of shallow spherical shells under uniform external pressure are solved by means of power series expansions following procedures introduced by Friedrichs and Stoker in their treatment of buckling of circular plates. These equations depend upon two parameters. One of these is related to the external pressure, while the other depends upon the dimensions of the shell. The equations are solved for several ranges of the parameters under boundary conditions corresponding to a fixed edge.

The solution, carried out numerically on the Univac at New York University, yields a complete description of the stresses and deflections as functions of the polar angle over a wide range of values of the loading parameter and the dimensional parameter. Prediction of the upper buckling load is then made by means of a numerical criterion based on the load vs deflection curve. For some cases, the post-buckling behavior is investigated. The results agree well with existing experimental and theoretical studies and cover a wide range of cases not previously treated.

TABLE OF CONTENTS

Page

Abstract.................................... 2

Symbols..................................... 4

Section

1. Introduction........................ 6

2. Derivation of Differential Equations..... 11

3. Technique of Solution................. 19

4. Computational Technique.............. 21

5. Discussion of Results................. 25

6. Post Buckling Behavior................ 31

7. Conclusions........................ 33

References.................................. 34

Appendix A.................................. 36

Table I..................................... 37

SYMBOLS

D = Flexural rigidity of shell $\dfrac{2Eh^3}{3(1-\nu^2)}$

E = Young's Modulus

F, G = Boundary functions, see Equation 19

$2h$ = Shell thickness

k = $2/3(1-\nu^2)$

N = Number of terms in power series required for convergence

p = External pressure, positive inwards

P = Loading parameter, see Equation 12

r = Radial variable: distance to any point in shell

R = Radius of middle surface of shell

S = Surface of shell

u = Tangential component of displacement

u^o = Tangential component of displacement on middle surface

V = Volume of shell

w = Radial component of displacement

w^o = Radial component of displacement on middle surface

$\bar{\alpha}$ = Slope of tangent plane to deformed surface with the horizontal plane

α = $\bar{\alpha}/\Lambda$

$\bar{\gamma}$ = Stress function, see Equation 10

γ = Reduced stress function, see Equation 12

$\varepsilon_{\bar{\theta}}$ = Longitudinal strain

$\varepsilon_{\bar{\Phi}}$ = Circumferential strain

ε = A small number

ε_{ij} = Components of strain tensor
ζ = R-r
η = A small number
$\bar{\theta}$ = Polar angle
θ = $\bar{\theta}/\Lambda$
Λ = Semi-angle of shell opening
λ = Kaplan and Fung geometric parameter
ν = Poisson's ratio
Π = Potential energy
ρ = Geometric parameter, see Equation 12
$\sigma_{\bar{\theta}}; \sigma^{0}_{\bar{\theta}}$ = Longitudinal stress; value on middle surface
$\sigma_{\bar{\varphi}}; \sigma^{0}_{\bar{\varphi}}$ = Circumferential stress; value on middle surface
τ^{ij} = components of stress tensor
$\bar{\varphi}$ = Azimuthal angle

Section 1. Introduction

Consider a thin, hollow sphere of wall thickness $2h$ and mean radius R loaded by a uniform external pressure p directed towards the center. It is observed experimentally that as the pressure increases from zero, the shell apparently deforms by contracting into a smaller sphere. This mode of deformation continues until some critical value of the pressure is reached. At this value the shell suddenly jumps, or buckles into a non-spherical buckled state consisting of a round, rotationally symmetric, inward "dimple" of small solid angle at some point on the surface of the shell, while the remainder of the shell remains apparently spherical.

These experimentally observed facts are entirely at variance with the linear theory of buckling[1]. Characteristically, the linear theory predicts a wave form extending over the whole surface, with the amplitude undetermined (e.g. the shell could buckle inward or outward under the same load). This is to be contrasted with the experimentally observed "dimpling" behavior. Furthermore, the experimental buckling load is found, in some cases, to be as low as one-quarter of that predicted by the linear buckling theory.

In a similar type of phenomenon observed in the case of buckling of thin cylindrical shells under axial compression, attempts were made to explain the discrepancy between theory and experiment on the basis of initial imperfections from the cylindrical shape of the model, and deviation of the boundary conditions from those assumed in the theoretical calculations. Although important, these effects were not sufficient to account for the lack of agreement (see the discussion in reference 2).

Von Karman and Tsien[2] recognized that this must be the result of a non-linear behavior of the structure. Based upon the minimization of a potential energy expression, they showed that for values of p below the buckling load predicted by the linear theory there exist other, non-adjacent, stable states of equilibrium. The greatest lower bound of such loads p is called the "minimum" or "lower" buckling load p_K. If p exceeds p_K there is a possibility that buckling will occur.

Friedrichs[3] pointed out some shortcomings, and suggested improvements in the Karman-Tsien theory. He also treated the buckling of a thin sphere as a "boundary layer" phenomenon where the "boundary layer" is considered as occuring in the dimpled region of the sphere. Tsien[4], adopting some of the suggestions of Friedrichs[3], presented an improved version of the Karman-Tsien[2] theory. Altshuler[5] attempted to determine the buckling load by solving the differential equations by asymptotic expansion techniques. Although none of these approaches are entirely satisfactory, they do reveal the essential nature of the phenomena that are involved in the buckling process.

Closely related to the problem of the buckling of a thin sphere is that of the buckling of a shallow[1] spherical shell under uniform external pressure. Physically as well as mathematically both problems reveal a similar non-linear behavior. The shallow spherical shell is of interest both as a structural entity in itself and as representing that portion of a complete sphere in which the dimpling occurs.

Solutions for the non-linear deformations of shallow spherical shells under various external pressures and edge moments have been obtained by Chien[12] and Feodosyev[13]. In reference [6] Kaplan and Fung present a theoretical and experimental treatment for the clamped shallow spherical shell under uniform external pressure. Their theoretical work is based upon a perturbation solution of the non-linear equations, where the non-dimensional radial deflection at the center of the shell serves as the perturbation parameter. Unfortunately, solutions to the resulting linear perturbation equations could be obtained only for very shallow shells. However, their experiments as observed in reference [7] revealed some new and interesting phenomena concerning the buckling of curved structures. Archer[15], using a similar set of equations derived by

---

[1] By shallow it is implied that the semi-angle of opening Λ of the spherical segment is a small angle; see Fig. 1.

Reissner[16], extended and improved the perturbation technique, and was able to obtain solutions for a greater range of shells than Kaplan and Fung. The agreement with experiments of the buckling loads predicted from the perturbation solutions becomes poorer as the value of the geometric shell parameter ($\rho = \frac{\lambda^2 R}{\sqrt{k}h}$) increases. Furthermore, the perturbation solution, based upon a one parameter expansion, fails to reveal the non-monotone dependence of buckling loads on ρ as indicated in reference [7]. Simons[14] proposes solving the non-linear equations[16] by a power series technique similar to that presented in this paper. His calculations however cover only a small range of parameters.

The physical problem that is treated in this paper is that of a thin, shallow spherical shell under the action of uniform external pressure. This shell is assumed fixed and clamped along the edge. Only rotationally symmetric deformations will be considered. The problem is considered as one in the non-linear theory of elasticity with small strains and small but finite deflections. Non-linear load vs deformation characteristics of the shell is expected to have the form shown in Fig. 2. Here, p represents the external pressure and w the radial deflection at some point, i.e. the center. Point A represents the "upper" or "initial" buckling load. Point B represents the "final" or "minimum" buckling load.

The present investigation has been successful in obtaining solutions including deflections and stresses for a large range of shell geometries for pressures from zero to those in the vicinity of point A of Fig. 2. Unfortunately only meagre results have been obtained so far for the "post-buckling" region, i.e. the portion of the curve A, B, C in Fig. 2.

The technique of solution employed was that of power series expansions inspired by the success of Friedrichs and Stoker[10], and Bromberg[11] in the problems of bending and buckling of circular plates. The use of this approach in the present problem, however, was only possible due to the availability of a high-speed digital computer.

Section 2. Derivation of Differential Equations

The non-linear equations for the deformation of spherical shells of small curvature, based upon an assumption of small strains and linear stress-strain law, were originally obtained by Chien[8] from static considerations. These equations can also be derived from a variational principle. In this case we employ the Principle of Minimum Potential Energy, and seek Euler's equations for the functional.

$$\Pi = \iiint_V \frac{1}{2} \tau^{ij} \varepsilon_{ij} dV + \iint_S p\, w\, d S \quad , \tag{1}$$

where: Π is the potential energy; τ^{ij} are the components of the stress tensor; ε_{ij} are the components of the strain tensor; w is the radial displacement; p is the external pressure, positive inwards. See Fig. 1 for the shell geometry.

The functional (1) may be expressed in terms of the components of displacement through the following relations.

Stress Strain

$$\tau^{11} \equiv \sigma_{\bar{\theta}} = \frac{E}{1-\nu^2}(\varepsilon_{\bar{\theta}} + \nu\varepsilon_{\bar{\varphi}}) \; ; \; \tau^{22} \equiv \sigma_{\bar{\varphi}} = \frac{E}{1-\nu^2}(\varepsilon_{\bar{\varphi}} + \nu\varepsilon_{\bar{\theta}}) \tag{2}$$

From the assumption of rotational symmetry all other stress and strain components vanish.

Strain Displacement

Let r be the radial distance to any point in the shell, and R the radius of the middle surface. The exact non-linear strain displacement relations for rotationally symmetric deformations in a spherical coordinate system, are then,

(3a) $$\varepsilon_{11} \equiv \varepsilon_{\bar{\theta}} = \frac{u_{\bar{\theta}} - w}{r} + \frac{1}{2}\left(\frac{w_{\bar{\theta}} + u}{r}\right)^2 + \frac{1}{2}\left(\frac{u_{\bar{\theta}} - w}{r}\right)^2$$

(3b) $$\varepsilon_{22} \equiv \varepsilon_{\bar{\phi}} = \frac{u \cot \bar{\theta} - w}{r} + \frac{1}{2}\left(\frac{u \cot \bar{\theta} - w}{r}\right)^2$$

where subscripts on u and w denote differentiation.

For the case of small finite deflections, u and w (analagous to the Foppl-Karman non-linear plate theory) and shallow shells (small $\bar{\theta}$, $u_{\bar{\theta}}^2$ is negligible compared to $u_{\bar{\theta}}$ and $w_{\bar{\theta}}^2$, and u is negligible compared to $w_{\bar{\theta}}$), equations (3a,b) reduce to

(4a) $$\varepsilon_{\bar{\theta}} = \frac{1}{r}(u_{\bar{\theta}} - w) + \frac{1}{2}\left(\frac{w_{\bar{\theta}}}{r}\right)^2$$

(4b) $$\varepsilon_{\bar{\phi}} = \frac{1}{r}\left(\frac{u}{\bar{\theta}} - w\right)$$

Equations (4a,b) are the strain displacement relations that will be employed in the variational expression. It is not clear to what extent these equations are adequate for non-shallow shells, without retaining additional terms from Equations (3a,b); for example, see page 260 of reference 3.

As is customary in thin shell theory the following assumptions are made concerning the distribution of the displacements through the shell thickness.

$$(5) \qquad u = u^{o} - \frac{\zeta}{R} w^{o}_{\bar{\theta}} \quad ; \quad w = w^{o}$$

where $\zeta = R-r$ and u^{o} and w^{o} are the displacements of the middle surface $\zeta = 0$.

Substituting (2), (4a,b) and (5) into (1), and performing the ζ and $\bar{\Phi}$ integrations, the potential energy Π may be written as,

$$\frac{\Pi}{2\pi R^2} = \int_{0}^{\Lambda} \frac{Eh}{1-\nu^2} ({\varepsilon^{o}_{\bar{\theta}}}^2 + {\varepsilon^{o}_{\bar{\Phi}}}^2 + 2\nu \varepsilon^{o}_{\bar{\Phi}} \varepsilon^{o}_{\bar{\theta}}) \, \bar{\theta} d\bar{\theta}$$

$$(6)$$

$$+ \int_{0}^{\Lambda} \frac{E}{3(1-\nu^2)} \frac{h^3}{R^4} [{w_{\bar{\theta}\bar{\theta}}}^2 \div \frac{1}{\bar{\theta}^2} w^2_{\bar{\theta}} + \frac{2\nu}{\bar{\theta}} w_{\bar{\theta}} w_{\bar{\theta}\bar{\theta}}] \, \bar{\theta} d\bar{\theta} + \int_{0}^{\Lambda} p w \bar{\theta}$$

where $\varepsilon^{o}_{\bar{\theta}}$ and $\varepsilon^{o}_{\bar{\Phi}}$ are the strains on the middle surface.

Setting the first variation of Equation (6) equal to zero, the following equilibrium equations result,

$$(7a) \qquad \sigma^{o}_{\bar{\Phi}} = \frac{d}{d\bar{\theta}} (\bar{\theta} \, \sigma^{o}_{\bar{\theta}})$$

$$-\frac{2h}{R}\left\{(\sigma^{o}_{\bar{\theta}} + \sigma^{o}_{\bar{\phi}})\bar{\theta} + \frac{1}{R}\frac{d}{d\bar{\theta}}(\bar{\theta}\, w_{\bar{\theta}}\, \sigma^{o}_{\bar{\theta}})\right\}$$

(7b)

$$+\frac{D}{R^4}\left\{\frac{d}{d\bar{\theta}}\,\bar{\theta}\,\frac{d}{d\bar{\theta}}\,\frac{1}{\bar{\theta}}\,\frac{d}{d\bar{\theta}}\,\bar{\theta}\, w_{\bar{\theta}}\right\} - p\bar{\theta} = 0 \quad ,$$

where $\sigma^{o}_{\bar{\theta}}$ and $\sigma^{o}_{\bar{\phi}}$ are stresses on the middle surface, and

$$D = \frac{2Eh^3}{3(1-\nu^2)} \quad .$$

Equations (7a,b) are a set of two equations in the three unknowns, $\sigma^{o}_{\bar{\theta}}$, $\sigma^{o}_{\bar{\phi}}$ and w. It is also necessary to satisfy the compatibility equation for the middle surface. This equation can be obtained by eliminating u from Equations (4a,b) for $r = R$. There results,

$$\text{(8)} \quad \frac{d}{d\bar{\theta}}\,\bar{\theta}(\sigma^{o}_{\bar{\phi}} - \nu\sigma^{o}_{\bar{\theta}}) - \sigma^{o}_{\bar{\theta}} + \nu\sigma^{o}_{\bar{\phi}} + \frac{E}{R}\,\bar{\theta}\, w_{\bar{\theta}} + \frac{E}{2}\left(\frac{w_{\bar{\theta}}}{R}\right)^2 = 0$$

In addition to yielding the differential equations (7a,b), the variational problem leads to the following boundary conditions

$$\Bigg[\frac{2h}{R}\,\sigma^{o}_{\bar{\theta}}\,\bar{\theta}\,\delta u^{o} + \frac{\bar{\theta}}{R^2}\left\{\frac{D}{R^2}\left(-\frac{d}{d\bar{\theta}}\,\frac{1}{\bar{\theta}}\,\frac{d}{d\bar{\theta}}\,\bar{\theta}\, w_{\bar{\theta}} + \nu w_{\bar{\theta}}\right) + 2h\sigma^{o}_{\bar{\theta}}\, w_{\bar{\theta}}\right\}\delta w$$

(9)

$$+\frac{D}{R^4}\left(\bar{\theta}\, w_{\bar{\theta}\bar{\theta}} + \nu w_{\bar{\theta}}\right)\delta w_{\bar{\theta}}\Bigg]_{0}^{\Lambda} = 0$$

The first equation of equilibrium (7a) is identically satisfied if we set

$$\sigma^{o}_{\bar{\theta}} = \frac{E}{2h} \frac{\bar{\gamma}}{\bar{\theta}} \quad ; \quad \sigma^{o}_{\bar{\phi}} = \frac{E}{2h} \bar{\gamma}_{\bar{\theta}} \quad . \tag{10a,b}$$

Furthermore, let us introduce the more convenient variables

$$\bar{a} = \frac{1}{R} \frac{dw}{d\bar{\theta}} + \bar{\theta} \tag{11}$$

and

$$\bar{a} = \Lambda a \quad ; \quad \bar{\theta} = \Lambda \theta \quad ; \quad k = \frac{2}{3(1-\nu^{2})}$$

$$\bar{\gamma} = (k)^{1/2} \frac{\Lambda h^{2}}{R} \gamma \quad ; \quad p = 2E(k)^{1/2} \left(\frac{h}{R}\right)^{2} P \quad ; \tag{12}$$

$$\rho = (k)^{-1/2} \Lambda^{2} \frac{R}{h}$$

Geometrically, the independent variable $\bar{a}$ defined in Equation (11) is the angle that the tangent plane to the deformed surface makes with the horizontal plane, see Fig. 1.

The parameter ρ, hereafter referred to as the "geometrical parameter", is proportional to the ratio of the shell rise and the thickness. The shell rise is defined as the height of the center of the shell above the horizontal plane through the edge. ρ is also roughly proportional to the ratio of membrane and bending stiffness. The relation between ρ and Kaplan and Fung's geometrical parameter λ is,

(12a) $$\rho = (2)^{-1/2} \lambda^2$$

Substituting (10a,b), (11) and (12) into (7a,b) and (8), and integrating (7b) once (employing the fact that from rotational symmetry $\frac{dw}{d\theta} = 0$ at $\theta = 0$) the following differential equations are obtained,

(13a,b) $$L\alpha = \rho(\alpha\gamma + P\theta^2) \ ; \quad L\gamma = \rho(\theta^2 - \alpha^2)$$

where L is the linear differential operator,

(14) $$L \equiv \theta \frac{d}{d\theta} \frac{1}{\theta} \frac{d}{d\theta} \theta \quad .$$

The boundary conditions corresponding to the differential equations (13a,b) are as follows: At the center, $\theta = 0$, from rotational symmetry

$$\alpha = 0 \quad ; \quad u = 0 \quad .$$

From Equations (2), (4a,b) and (10a,b) this is equivalent to

(15) $$\alpha(0) = 0 \quad ; \quad \gamma(0) = 0 \quad .$$

At the edge, $\theta = 1$, we assume that the plate is held fixed and clamped. This condition can also be considered as simulating the boundary separating the region of dimpling from that of uniform contraction of a complete sphere. Therefore, the conditions are

$$\alpha = 1 \quad ; \quad u = 0 \quad ; \quad w = 0$$

This is equivalent to

$$\alpha(1) = 1 \quad ; \quad \left. \gamma_\theta - \nu\gamma \right]_{\theta=1} = 0 \tag{16}$$

It should be observed that if conditions (15) and (16) are imposed then the boundary conditions (9), resulting from the variational problem, are identically satisfied.

Thus, the complete formulation of the problem consists of the differential equations (13a,b) subject to the boundary conditions (15) and (16). These equations— a pair of second order, coupled, ordinary, non-linear differential equations —are quite similar to the equations governing the non-linear deflections of circular plates,[9,10,11] except for the addition of extra terms resulting from the initial curvature. However the physical phenomena that these equations describe are quite different. Mathematically, the buckling problem for the circular plate, or the bending problem differ in their parametric dependence from the spherical shell problem. The plate problems depend upon one parameter, either a reduced edge load (the "thrust ratio", see Reference [10]) or a reduced lateral load, see Reference [11]. While on the other hand, the equations governing the shell problem depend upon two parameters, P and ρ. From this point of view, it would seem that to obtain a more reasonable perturbation solution, for the shell problem a two parameter expansion should be attempted.

Section 3. Technique of Solution

The technique of solution to be employed for the boundary value problem posed by Equations (13a,b), (15), and (16) is to expand the dependent variables α and γ in power series in θ. This approach has been used in non-linear circular plate problems by Way[9], Friedrichs and Stoker[10] and Bromberg[11].

From (13a,b) and the boundary conditions at $\theta = 0$ the power series for α and γ must contain odd powers only so that

$$(17) \qquad \alpha = \sum_{n=1}^{\infty} \alpha_n \theta^{2n-1} \; ; \quad \gamma = \sum_{n=1}^{\infty} \gamma_n \theta^{2n-1} \quad .$$

By substitution of these power series into (13a,b) the following recurrence relations for the coefficients α_n and γ_n are obtained.

$$(18) \quad \begin{cases} \alpha_2 = \rho/8(\alpha_1\gamma_1 + P) \; ; \quad \gamma_2 = \rho/8(1 - \alpha_1^2) \; ; \\ \text{for} \quad n > 2 \\ \alpha_n = \dfrac{\rho}{4n(n-1)} \displaystyle\sum_{i=1}^{n-1} \alpha_i \gamma_{n-i} \; ; \quad \gamma_n = - \dfrac{\rho}{4n(n-1)} \displaystyle\sum_{i=1}^{n-1} \alpha_i \alpha_{n-i} \end{cases}$$

Again, by insertion of the power series into Equation (16) the boundary conditions at $\theta = 1$ can be written as

$$\sum_{n=1}^{\infty} \alpha_n = 1 \quad ; \quad \sum_{n=1}^{\infty} (2n-1-\nu)\gamma_n = 0 \quad .$$

Since it is possible, through the recurrence relations (18), to express all α_n and γ_n in terms of α_1 and γ_1 the above conditions constitute a pair of simultaneous equations in α_1 and γ_1 i.e.

$$(19) \quad F(\alpha_1,\gamma_1) \equiv \sum_{n=1}^{\infty}\alpha_n - 1 = 0 \; ; \; G(\alpha_1,\gamma_1) \equiv \sum_{n=1}^{\infty}[2n-(1+\nu)]\gamma_n = 0 \; .$$

The problem thus reduces, for given P and ρ, to solving the two simultaneous equations (19) for the unknowns α_1 and γ_1. Once the root or roots of these equations are obtained all the α_n and γ_n and hence all the stresses and displacements are then determined; (see Appendix A).

Section 4. Computational Technique

The computational problem is, for a given set of parameter values (P,ρ) to determine the roots (α_1,γ_1) satisfying (19). For computing purposes, it is necessary to replace the exact equations (19) by the approximate conditions

$$(19') \quad |F(\alpha_1,\gamma_1)| \doteq \left|\sum_{n=1}^{N} \alpha_n - 1\right| < \eta \ ; \quad |G(\alpha_1,\gamma_1)| \doteq \left|\sum_{n=1}^{N} [2n-(1+\nu)]\gamma_n\right| <$$

where η is a small number and N is an integer determined on the basis of a convergence criterion for the series. In the majority of the computations η was chosen as 1×10^{-4}. N is never greater than 99.

For a fixed P and ρ the procedure starts from a reasonable guess for (α_1,γ_1), say $(\alpha_1,\gamma_1)^0$. Then from (18) α_n and γ_n corresponding to $(\alpha_1,\gamma_1)^0$ are computed for $n \leq N$. As a convergence criterion for the series (17), it is prescribed that the sum of the absolute magnitudes of the last three computed α_n and γ_n be less than a certain small number, ε. That is, the computation of α_n and γ_n in (18) ceases for $n = N$ such that

$$(20) \quad |\alpha_N|+|\alpha_{N-1}|+|\alpha_{N-2}|<\varepsilon \ ; \quad |\gamma_N|+|\gamma_{N-1}|+|\gamma_{N-2}|<\varepsilon \ .$$

In the majority of the computations ε was set equal to 1×10^{-4}.

When the α_n and γ_n satisfy Equation (20), they are inserted into the expressions for $F(\alpha_1, \gamma_1)$ and $G(\alpha_1, \gamma_1)$. If F and G satisfy Equation (19'), the stress and displacement distribution throughout the shell are computed from the relations listed in Appendix A. In general, however, F and G do not satisfy Equation (19'), and it is necessary to obtain an improved approximation to (α_1, γ_1). This is done systematically by means of the Newton-Raphson iteration process. The partial derivatives of F and G in the Newton-Raphson process are approximated by forward difference quotients. This iteration process is repeated until Equation (19') is satisfied. The displacements and stresses are then computed from the equations of Appendix A. The number of iterations required for convergence varies with the (P, ρ) selection and the initial guess $(\alpha_1, \gamma_1)^o$. For most of the cases encountered, two to six Newton-Raphson iterations were necessary. The number of coefficients, N, that were required for convergence varied with the (P, ρ) selection; Table I gives some representative values. The computation of coefficients, the iteration process, and the calculation of stresses and displacements are all performed on the Univac at New York University.[1]

The method for calculating with fixed P and ρ has thus been described. The computations proceed, for fixed ρ, by obtaining a sequence of roots (α_1, γ_1) for a corresponding sequence of increasing values of P. A first guess for (α_1, γ_1) is determined by selecting a low value for P, usually $P = .1$. For such low values of P the deformed state, and hence the first (α_1, γ_1) guess, should be nearly spherical. The Newton-Raphson process then rapidly yields the root (α_1, γ_1) to the required accuracy. The initial guess of the roots for successivly higher values of P is obtained by extrapolation of the preceding roots in the sequence. This is done with the aid of a plot of α_1 vs γ_1 as shown in Fig. 3. This procedure is terminated for either of two reasons: the Newton-Raphson iteration process fails to converge to a root in a large number of iterations (usually 10); or the coefficients fail to converge according to Equation (20). As an example of the first reason for termination, with $\rho = 32$ and $P = 1.25$ the procedure converged in 3 iterations. However, with $P = 1.3$ there was no indication of convergence in 10 Newton-Raphson iterations. An illustration of the second reason for termination is for $\rho = 26.1$ and $P = 1.55$. Here convergence occured in 2 iterations and 40 terms of the power series. But, for $P = 1.6$, 99 terms were computed with Equation (20) not being satisfied. In fact, the terms were steadily growing in absolute magnitude.

---

[1] The authors are indebted to Miss M. Weissner and Messrs. A. Paster and S. B. Weinberg for their aid in coding and programming this problem.

The criterion for the initial buckling that is used in this investigation is based on this terminating value of P. Direct application of the "classical" criterion (the load at which $\frac{dP}{dw} = 0$) for buckling seems impracticable with the present technique of solution. Instead, the numerical equivalent of the buckling phenomena is used as the criterion for determining the buckling load, i.e. the failure of the computing process to produce a neighboring solution corresponding to a small increment in the load. If P_1 represents the last value of P for which convergence occurs, and P_2 represents the next value of P attempted, then the initial buckling load, P_{cr}, is assumed to lie in the interval $P_1 \leq P_{cr} \leq P_2$.

Section 5. Discussion of Results

Before proceeding to a discussion of the results of our calculations, a brief review of the experimental results of Kaplan and Fung[6] and the interpretation given in reference [7] will be presented.

Kaplan and Fung constructed a series of shallow spherical domes of varying radii and thickness. These domes were placed in a clamping jig and loaded under uniform external pressure. In addition to measuring the initial and final buckling pressures, they measured the vertical deflections at various points for several different values of the pressure.

For low values of the geometric parameter ρ (or equivalently Kaplan and Fung's λ as related by **Equation** 12a) the experiments showed that the form of the deflections are such that the maximum deflection is at the center of the shell, and decreases steadily toward the edge. This will be called mode of deformation I. As ρ increases, it was observed that the peak deflection at the center gradually flattened out, until at ρ equal approximately 21, the maximum deflection occurs at some point between the center and edge; so that there is also a local minimum point at the center. This will be called mode of deformation II. With a further increase in ρ the maximum point moved toward the edge until approximately $\rho = 55$. Then the shell deformed in a third mode. This mode has two local maximum points, one at the center and the other between the center and the edge, see Fig. 16 of Reference 6.

When the experimental buckling loads are plotted against ρ rather than λ, it is found[7] that there is an interesting peaking behavior in these loads as a function of ρ, see Fig. 4. In Fig. 4 the crosses and circles indicate the experimental values of Kaplan and Fung, while the solid line indicates the apparent trend of the experimental data. It is significant to note that these peaks in the buckling loads occur at those values of ρ at which a change of mode of deformation had been observed.

In proceeding with our numerical solutions on the Univac we have in a real sense conducted "experiments" on shallow spherical shells. For each given value of ρ (i.e. a particular shell configuration) deflection and stress "measurements" are made for increasing values of load P. As in a physical experiment, the initial buckling load is considered to be reached, when for a small increment in P no neighboring solution to the previously attained solution can be found, i.e. the iteration process suddenly fails to converge.

For low values of ρ, $\rho < 23$, the numerical results confirm Kaplan and Fung's experiments. In Figures 5a,b,c,d are plotted some values of the deflections and stresses as a function of θ. The plots are for increasing load P at a constant value of ρ. In this case $\rho = 11.312$ was selected as representative of the mode of deformation of type, or region I. In Fig. 5a the radial deflection w can be seen to peak at the center and fall off towards the edge. The dotted lines indicating the results from the perturbation solution of Kaplan and Fung[6]. It can also be noted from Figures 5b,c,d that the stresses exhibit a similar behavior.

For increasing values of ρ, the graphs of these functions tend to flatten out in the central region of the shell $(\theta = 0)$. This process continues until $\rho = 23.5$, see Fig. 6 where only the results for the radial deflection are presented. For this value of ρ and for low values of load, say $P \leq .4$, the shell deforms in mode I with maximum deflection at the center. However, for higher load the mode of deformation gradually changes into type II, with the maximum deflection located somewhere between the center and the edge (in this case $\theta \approx .3$). It is to be noted from Fig. 4 that the shell $\rho = 23.5$ falls in the peaking region of the buckling loads. Thus, the mode of deformation for constant ρ may change with increasing load. This clearly illustrates the two parameter dependence of the character of the solutions.

In Figures 7a,b,c,d are shown plots of deflections and stresses for a typical shell $\rho = 32$, of mode II of deformation for increasing values of load. Notice, that the longitudinal membrane stress Fig. 7b also has a maximum located between the center and edge (compare to Fig. 5b). The behavior of the bending stresses for mode II (see Figures 7c,d), shows a marked difference from that of mode I (see Figures 5c,d). For mode I, the bending stresses fall off in a smooth manner from the center to the edge, while for mode II there is a local minimum near $\theta = .6$ and then the stresses change rapidly towards the edge. This is reminiscent of the boundary layer phenomenon found by Friedrichs and Stoker[10] for the buckling of circular plates.

A further increase in ρ results in a flattening of the deflection and stress distributions in the central portion of the shell, and a movement of the maximum point towards the edge. Mode II persists until $\rho \approx 52$ when a transition case similar to $\rho = 23.5$ is detected. However this time the transition is from mode II to mode III. In the radial deflection plot, the mode III form is barely visible. However it can clearly be observed in the bending stress graphs. It is not until large ρ, say $\rho = 176$, that there is a sharp appearance of mode III in the radial deflection graph, (see Fig. 8). Again from Fig. 4 it can be observed that the transition of modes occurs at the peaking of the buckling loads.

In Figures 9a,b,c,d the deflections and stresses are again plotted against θ, but this time for constant P and increasing ρ. In Fig. 9a the motion of the maximum deflection point towards the edge with increasing ρ is clearly indicated. This is again reminiscent of boundary layer phenomena. In the plots for the longitudinal membrane stress (Fig. 9b) and in particular the bending stresses (Fig. 9c,d) the change in mode shape is clearly illustrated.

The load vs deflection at the center characteristics for various values of ρ are plotted in Fig. 10 and compared with the theoretical and experimental results obtained by Kaplan and Fung. For low values of ρ the agreement with the experiments is only fair, while for increasing ρ the agreement between the physical and numerical experiments becomes uniformly better. This is probably caused by the fact that for shallow shells (small ρ) the effect of initial imperfections are more pronounced, and that the shallower the shell the more difficult it is to properly measure the radius.

Initial Buckling Loads: The results of the numerical computation of P_{cr} as well as the experimental results of Kaplan and Fung are presented in Fig. 4. The intervals, $P_1 P_2$, in which the P_{cr} lie are indicated by short vertical lines. It can be observed that the computed P_{cr} follow the same general trend as the experimental data, indicating a peaking behavior as a function of ρ. The agreement between experiment and theory is least satisfactory in the region of peaking $[18 \leq \rho \leq 25, 50 \leq \rho \leq 60]$. In this region a small error in the experimental determination of ρ may lead to a large error in P_{cr} for a particular shell. It can also be observed from Fig. 4 that in some cases the numerical results predict greater P_{cr} than the experiments, while in other cases it is just the opposite. There is no apparent trend in this respect.

Section 6. Post Buckling Behavior

The post-buckling region is defined as the region A,B,C, of Fig. 2, i.e. the behavior of the shell after $P = P_{cr}$. The primary purpose of investigating this region is to determine the lowest value of P,($P = P_B$) for which there exist non-unique solutions to the boundary value problem described by Equations (13a,b), (15) and (16). The procedure previously outlined does not enable us to continuously obtain solutions beyond point A. However, starting from a solution in the neighborhood of point C we may apply the previous procedure with a decreasing sequence of P values to obtain the point B.

To obtain a solution in the neighborhood of point C we select a sufficiently large value of P (say P = 2.2). For a "flat" shell the load vs deformation characteristics must be monotone; i.e. there is no buckling. Therefore for a sufficiently small value of ρ it is possible to obtain a solution, using the previous procedure, for this value of P. Then starting with the solution for this value of ρ we obtain a sequence of solutions for an increasing sequence of ρ values and fixed P (see Fig. 11, ρ = .8, 4.8, 6.4, 7.24). This procedure is analogous to the original procedure where the roles of P and ρ are interchanged.

We note how for increasing ρ values the characteristics depart more and more from the initial linear relation and approach the buckling type curve.

A solution is thus obtained for $P = 2.2$ and $\rho = 11.312$. This load is higher than that previously used and corresponds to much larger deflections. Keeping ρ fixed a decreasing sequence of P values is selected in an attempt to locate point B. Unfortunately, convergence of the computations becomes increasingly poor as P decreases. Solutions are obtained only for the range $1.8 \leq P \leq 2.2$, see Fig. (11). The initial portion of the curve for $\rho = 11.312$ is also shown in Fig. 11. Fig. 12 represents the radial deflection over the shell for one value of P in the post-buckling region.

Section 7. Conclusions

Numerical solutions of the non-linear equations governing the deflections of clamped shallow, spherical shells under a uniform external pressure have been obtained by power series technique. The computations were conducted on the Univac at N. Y. U. These solutions yield stress and deflection distributions over the shell as well as estimates of the initial buckling loads for a wide range of values of the shell parameters. The two parameter dependence of the solutions and the various modes of deformation have been clearly shown. Only a limited number of solutions for the post-buckling region have been obtained. It is anticipated that some improvements in the numerical method may yield additional results in this region.

The authors wish to express their appreciation to Professor J. J. Stoker for suggesting this investigation.

REFERENCES

[1] Timoshenko, S., Theory of Elastic Stability, McGraw-Hill Book Co., New York, 1936.

[2] von Karman, T. and Tsien, H. S., The Buckling of Spherical Shells by External Pressure, Journal of the Aeronautical Sciences, Vol. 7, No. 2, pp. 43-50, December, 1939.

[3] Friedrichs, K. O., On the Minimum Buckling Load for Spherical Shells, von Karman Anniversary Volume, pp. 258-272, California Institute of Technology, Pasadena, 1941.

[4] Tsien, H. S., A Theory for the Buckling of Thin Shells, Journal of the Aeronautical Sciences, Vol. 9, No. 10, pp. 373-384, August, 1942.

[5] Altshuler, B., Non-Linear Buckling of a Spherical Shell, Doctoral Thesis, New York University, 1953.

[6] Kaplan, A., and Fung, Y. C., A Non-linear Theory of Bending and Buckling of Thin Elastic Shallow Spherical Shells, NACA TN 3212, 1954.

[7] Reiss, E. L., On the Non-linear Buckling of Shallow Spherical Domes, Journal of the Aeronautical Sciences, Vol., 23, No. 10, pp. 973-975, October, 1956.

[8] Chien, W. Z., The Intrinsic Theory of Thin Shells and Plates, Quar., of Appl. Math., Vol. II, No. 2, pp. 120-135, July, 1944.

[9] Way, S., Bending of Circular Plates With Large Deflection, Trans. A. S. M. E., Vol. 56, p. 627, 1934.

[10] Friedrichs, K. O., and Stoker, J. J., The Non-linear Boundary Value Problem of the Buckled Plate, Amer. Jour. of Math., Vol. LXIII, No. 4, pp. 839-888, October, 1941. Buckling of the Circular Plate Beyond the Critical Thrust, Jour. of Appl. Mech., Vol. 9, No. 1, pp. A7-A14, March, 1942.

[11] Bromberg, E., Non-linear Bending of a Circular Plate Under Normal Pressure, Doctoral Thesis, New York University, 1950.

[12] Chien, W. Z., and Hu, H. C., On the Snapping of a Thin Spherical Cap, paper presented before IX International Congress of Applied Mechanics, Brussels, Bel., September, 1956.

[13] Feodosyev, V. I., On the Stability of a Spherical Shell Under the Action of an External Uniform Pressure, (In Russian), Prikl. Mat. Mek., Vol. 18, No. 1, pp. 35-42, 1954.

[14] Simons, R. M., A Power Series Solution of the Nonlinear Equations for Axi-Symmetrical Bending of Shallow Spherical Shells, Jour. Math. and Phy., Vol. 35, No. 2, pp. 164-176, 1956.

[15] Archer, R. R., Stability Limits for a Clamped Spherical Shell Segment Under Uniform Pressure, Doctoral Thesis, Mass. Inst. of Tech., May, 1956.

[16] Reissner, E., On Axi-Symmetrical Deformations of Thin Shells of Revolution, Proc. of Symp. on Appl. Math., Amer. Math. Soc., Vol. 3, p. 27, 1950.

APPENDIX A

Once the roots (α_1, γ_1) are obtained for a given set of parameter values (P, ρ), the stresses and deflections may be computed from the following relations:

(A1) $$\alpha(\theta) = \sum_{n=1}^{N} \alpha_n \theta^{2n-1}$$

(A2) $$\frac{w(\theta)}{\rho h\sqrt{k}} = \frac{1}{2}[1 - \sum_{n=1}^{N} \frac{\alpha_n}{n} + \sum_{n=1}^{N} \frac{\alpha_n}{n} \theta^{2n} - \theta^2]$$

(A3) $$\frac{w(0)}{\rho h\sqrt{k}} = \frac{1}{2}(1 - \sum_{n=1}^{N} \frac{\alpha_n}{n})$$

Membrane stresses: $\bar{\sigma} = \frac{\sigma}{E}$

(A4) $$2(k)^{-1/2} \frac{R}{h} \bar{\sigma}_\theta^o = \sum_{n=1}^{N} \gamma_n \theta^{2n-2}$$

(A5) $$2(k)^{-1/2} \frac{R}{h} \bar{\sigma}_\phi^o = \sum_{n=1}^{N} (2n-1)\gamma_n \theta^{2n-2}$$

Bending stresses: at upper and lower surfaces

(A6) $$\frac{R}{h} \bar{\sigma}_\theta \Big|_{\mp h} = \frac{\sqrt{k}}{2} \sum_{n=1}^{N} \gamma_n \theta^{2n-2} \pm (1-\nu^2)^{-1} [\sum_{n=1}^{N} (2n-1+\nu)\alpha_n \theta^{2n-2} - (1+\nu)]$$

(A7) $$\frac{R}{h} \bar{\sigma}_\phi \Big|_{\mp h} = \frac{\sqrt{k}}{2} \sum_{n=1}^{N} (2n-1)\gamma_n \theta^{2n-2} \pm (1-\nu^2)^{-1} [\sum_{n=1}^{N} (2\nu n+1-\nu)\alpha_n \theta^{2n-2} - (1+\nu)]$$

TABLE I

The Number N, of Coefficients Required for Convergence

ρ	P			
	.2	.8	1.0	1.4
12.23	11	13	14	19
17.22	13	17	19	23
32.0	16	26	31	X
52.2	20	36	46	X
64.0	22	42	54	X

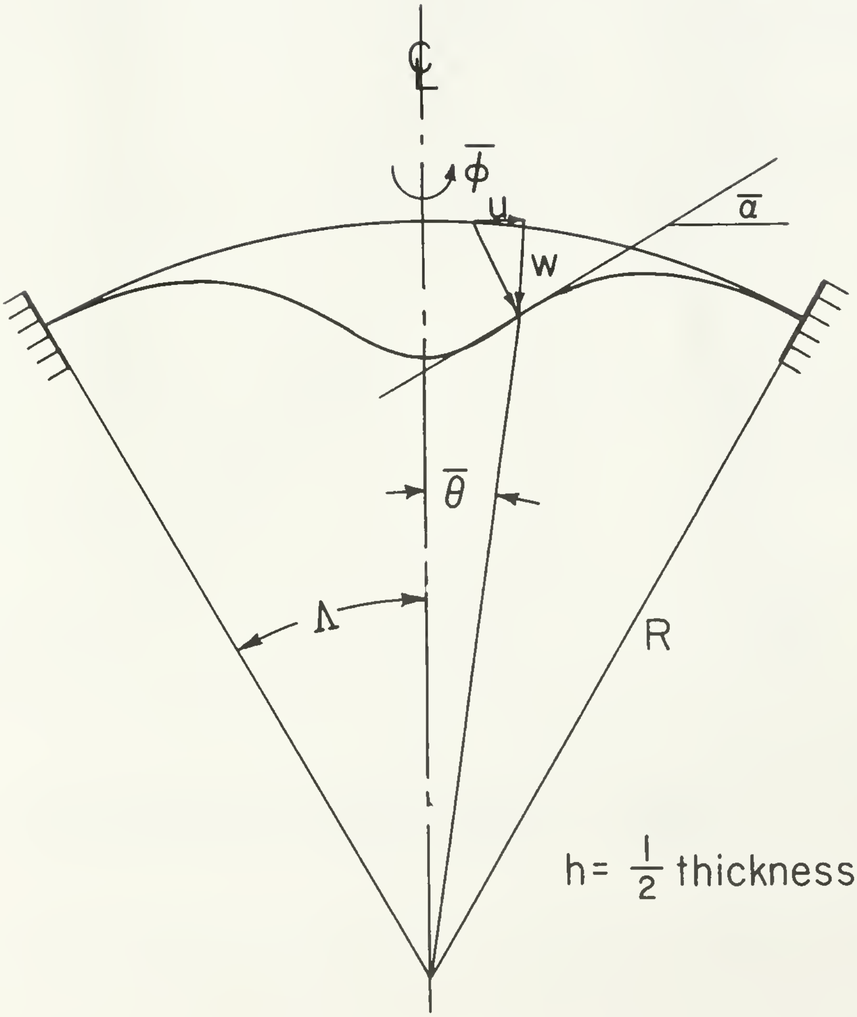

SHELL GEOMETRY

Fig. 1

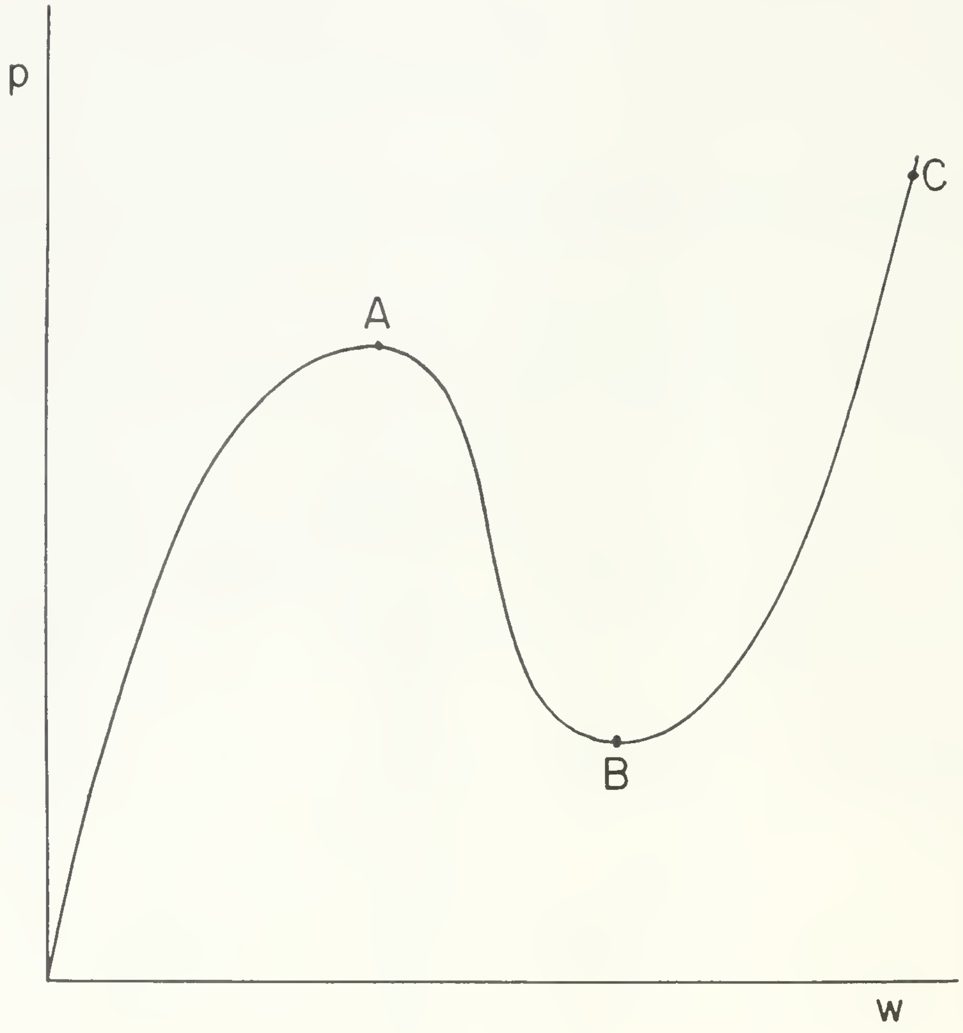

Load vs Deformation Characteristics

Fig. 2

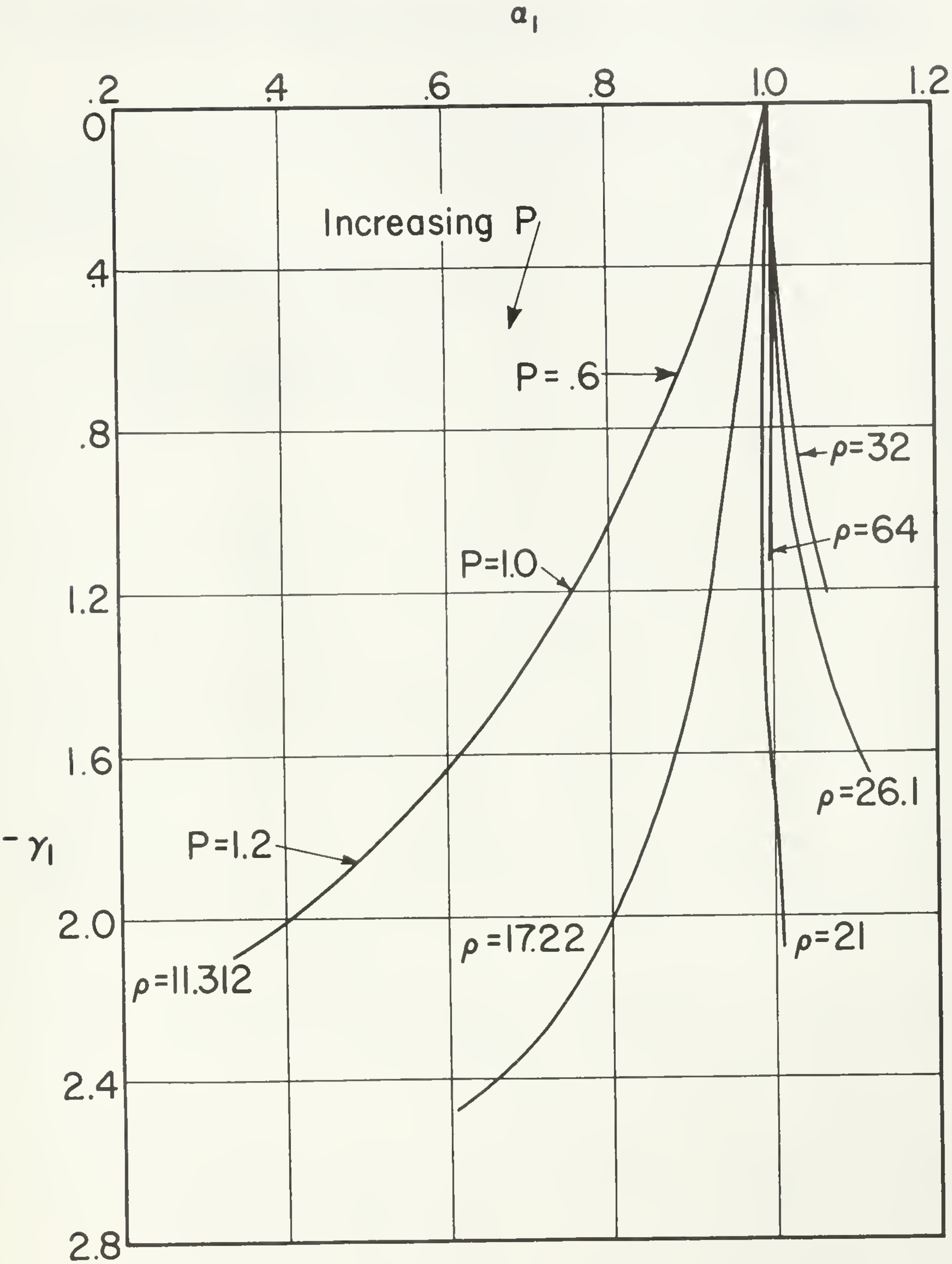

α_1, γ_1 PLANE

Fig. 3

COMPARISON OF THEORETICAL AND EXPERIMENTAL INITIAL BUCKLING LOADS

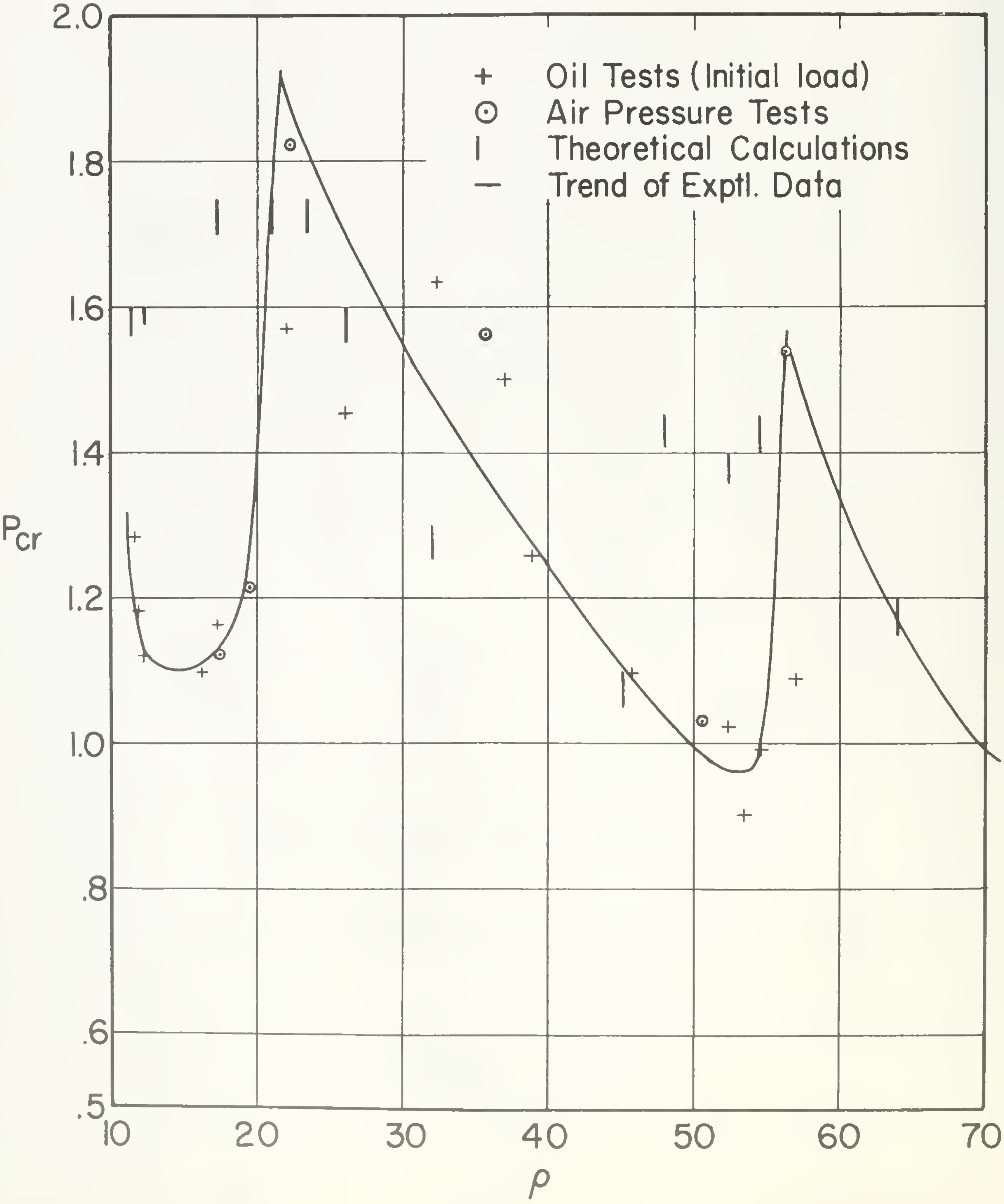

Fig. 4

REDUCED RADIAL DEFLECTION

$\rho = 11.312$ REGION I

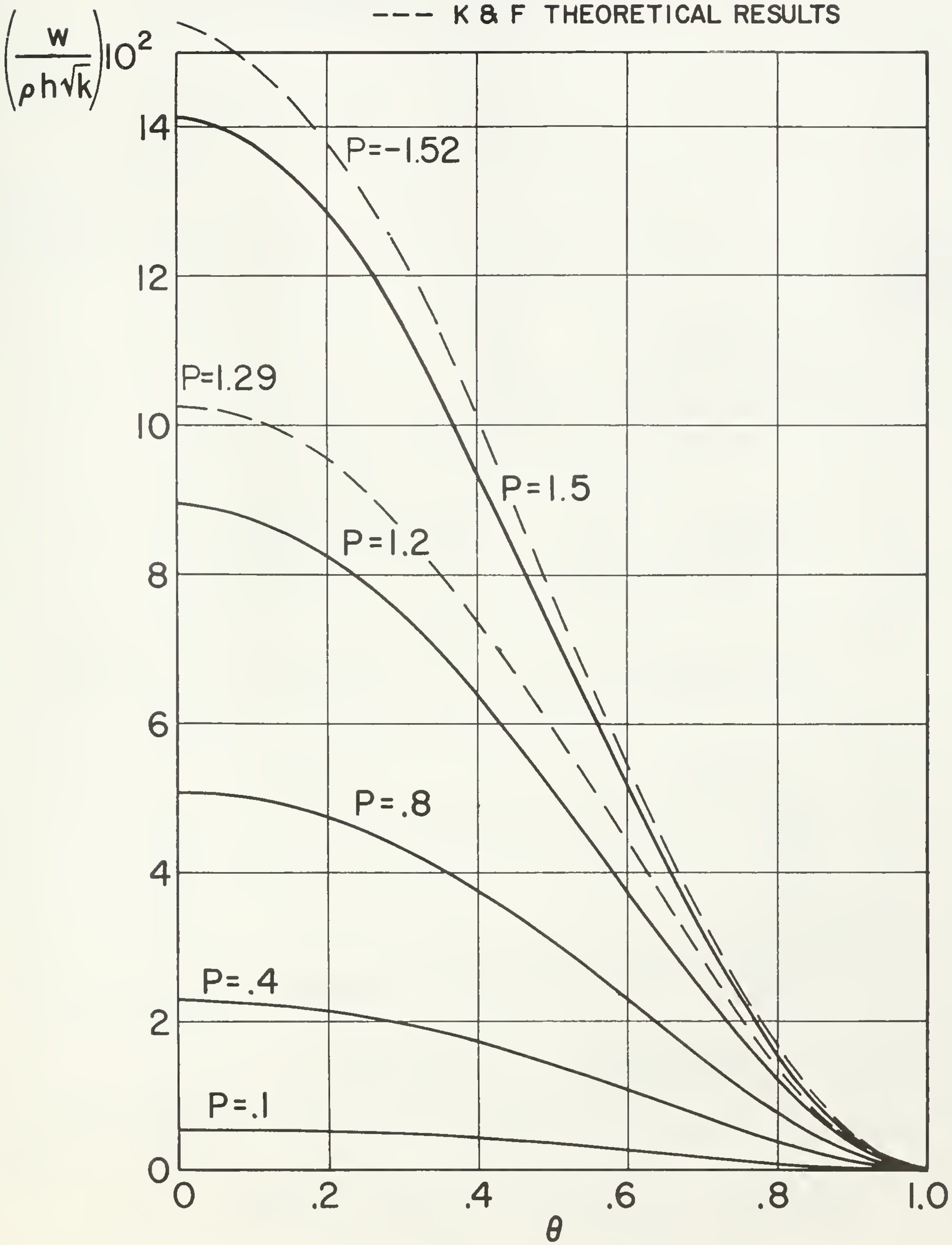

Fig. 5a

REDUCED LONGITUDINAL STRESS

$\rho = 11.312$ REGION I

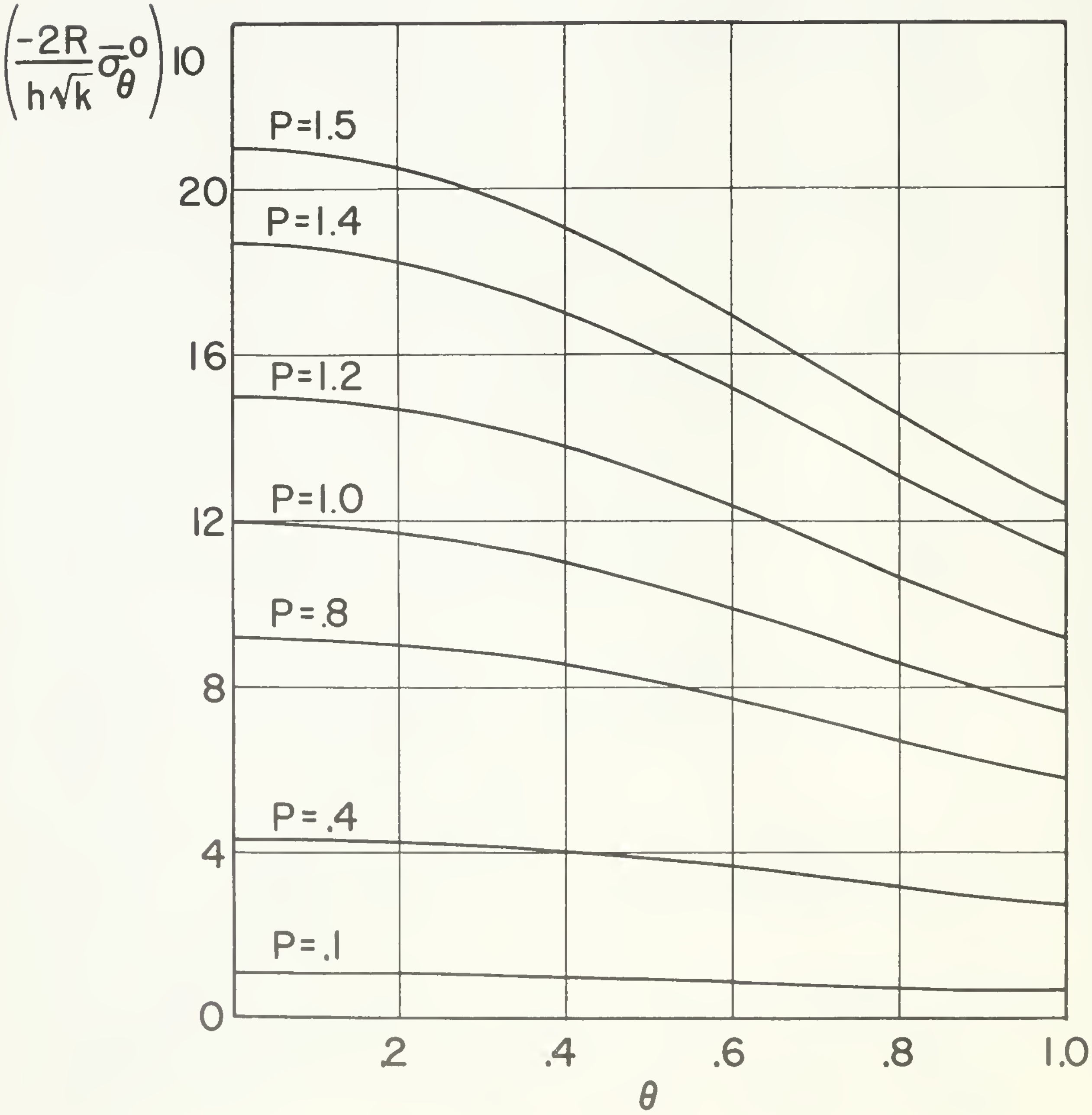

Fig. 5b

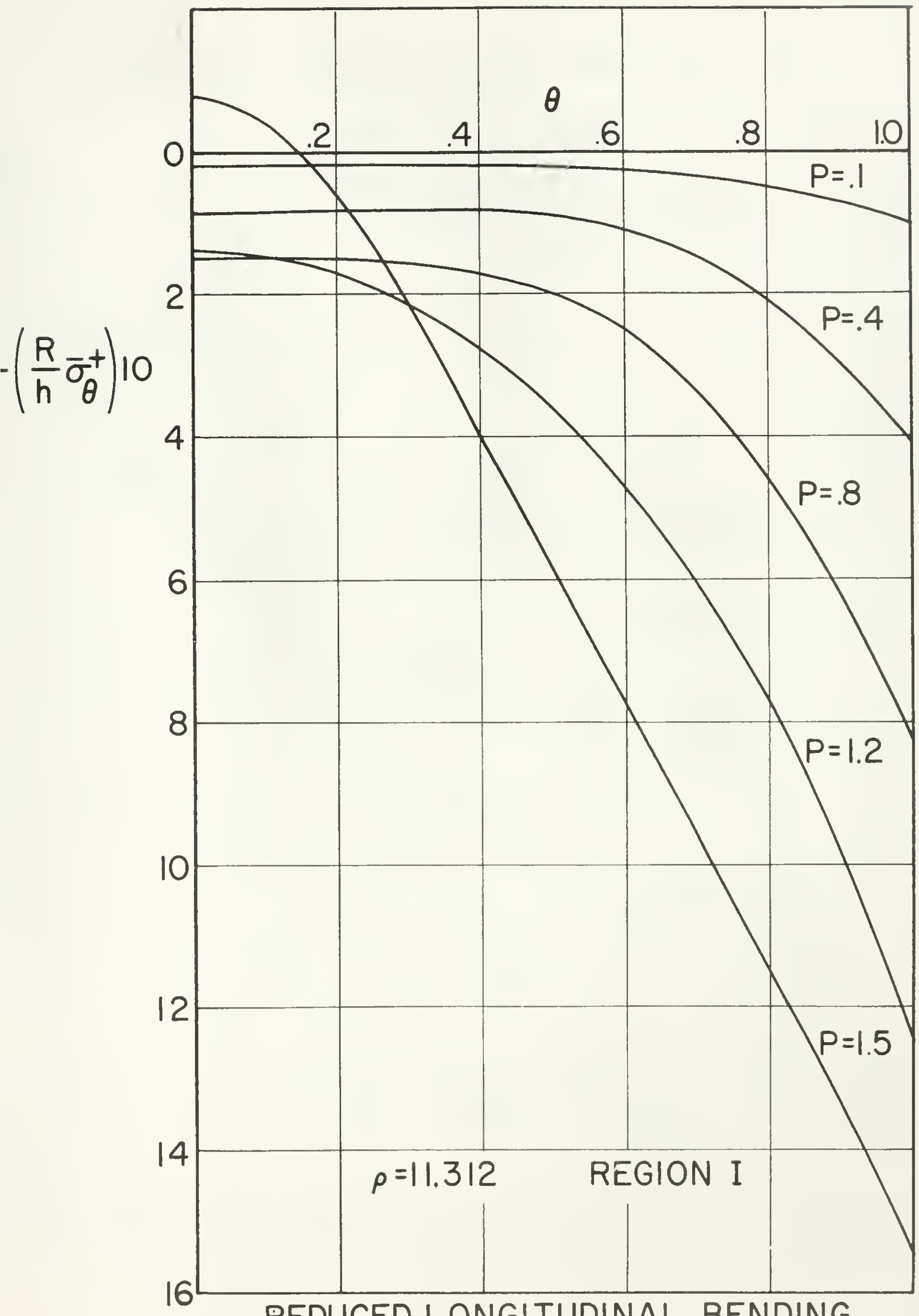

REDUCED LONGITUDINAL BENDING

STRESS — TOP SURFACE

Fig. 5c

REDUCED LONGITUDINAL BENDING STRESS — BOTTOM SURFACE

$\rho = 11.312$ REGION I

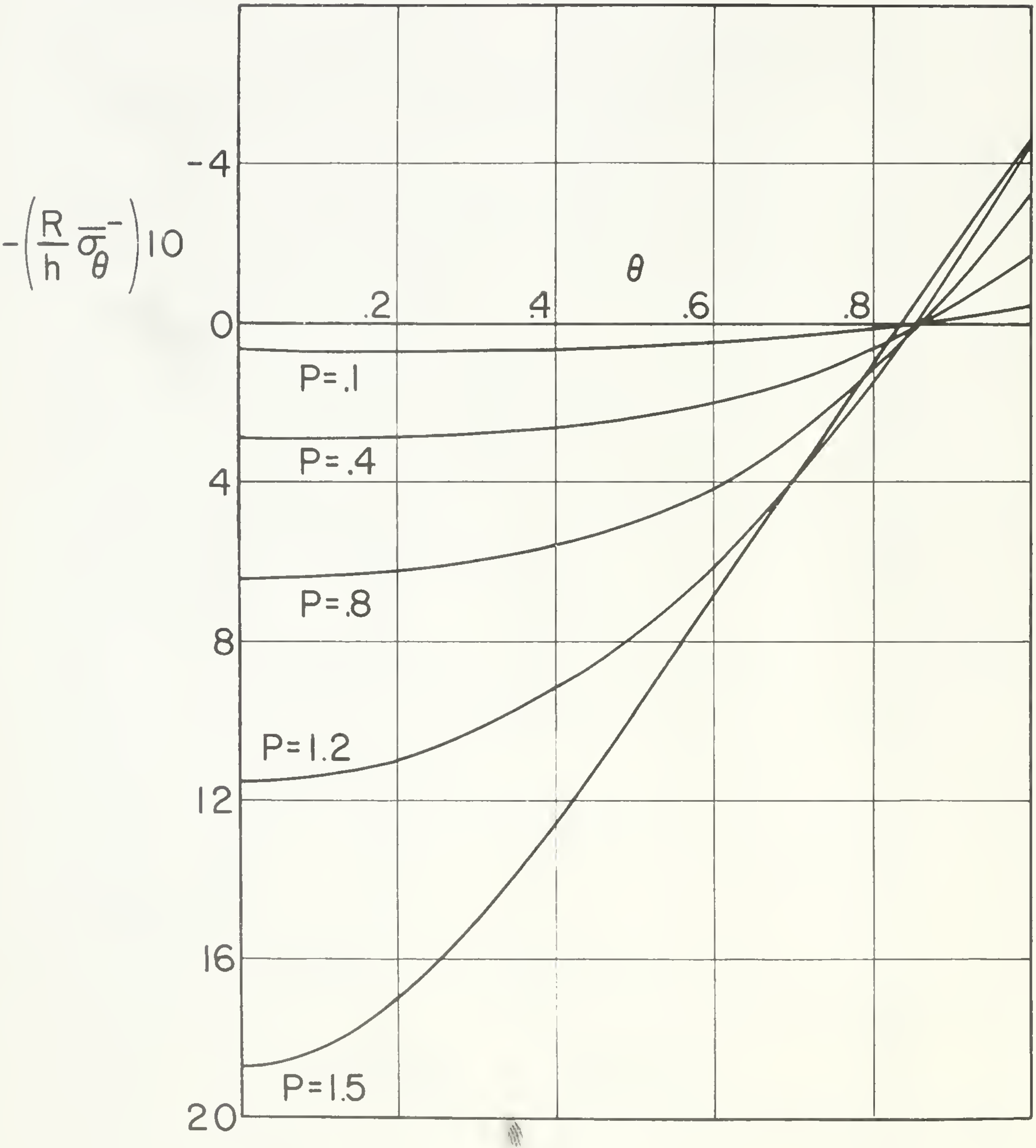

Fig. 5d

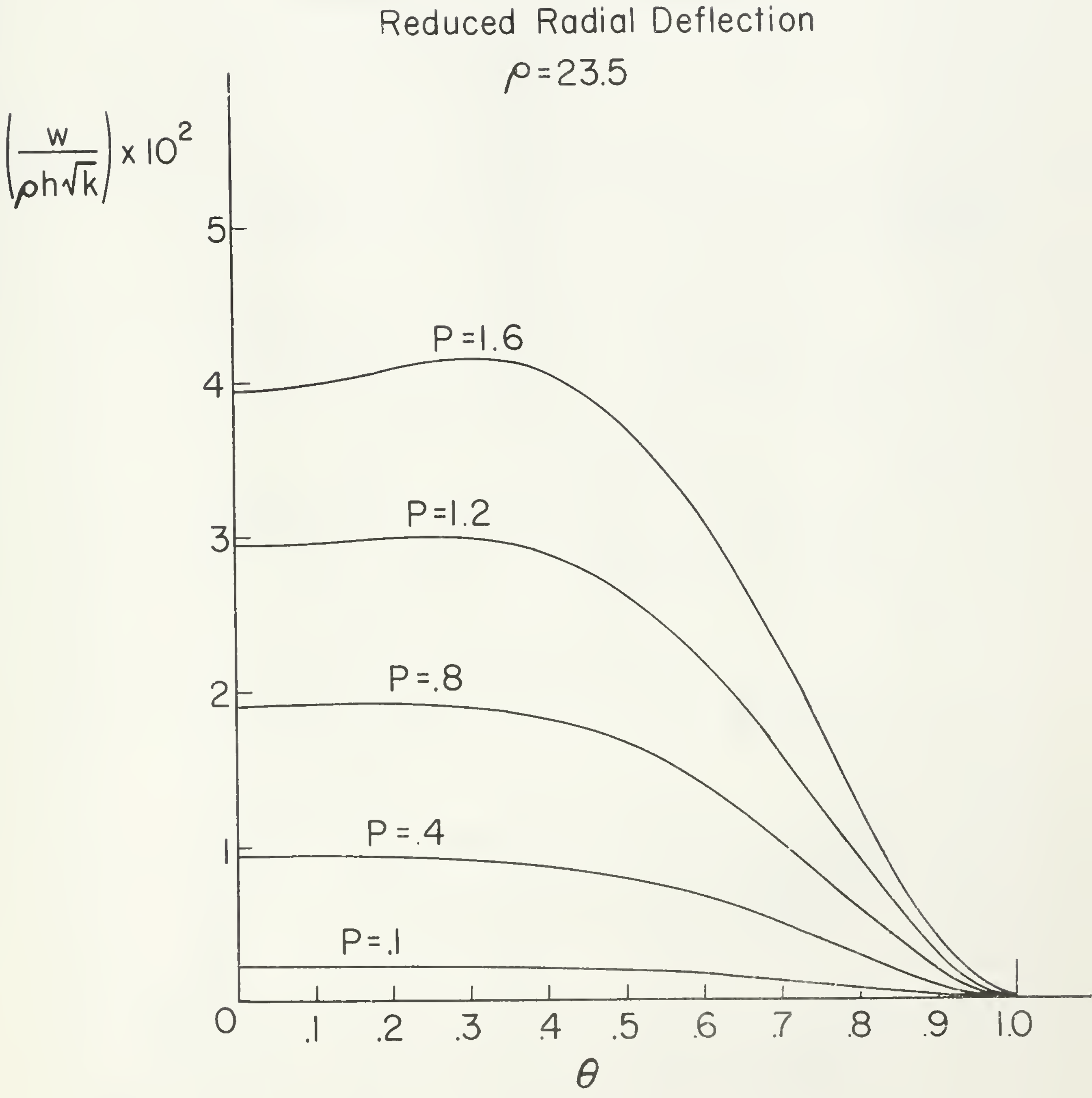

Reduced Radial Deflection

$\rho = 23.5$

Fig. 6

REDUCED RADIAL DEFLECTION

$\rho = 32$ REGION II

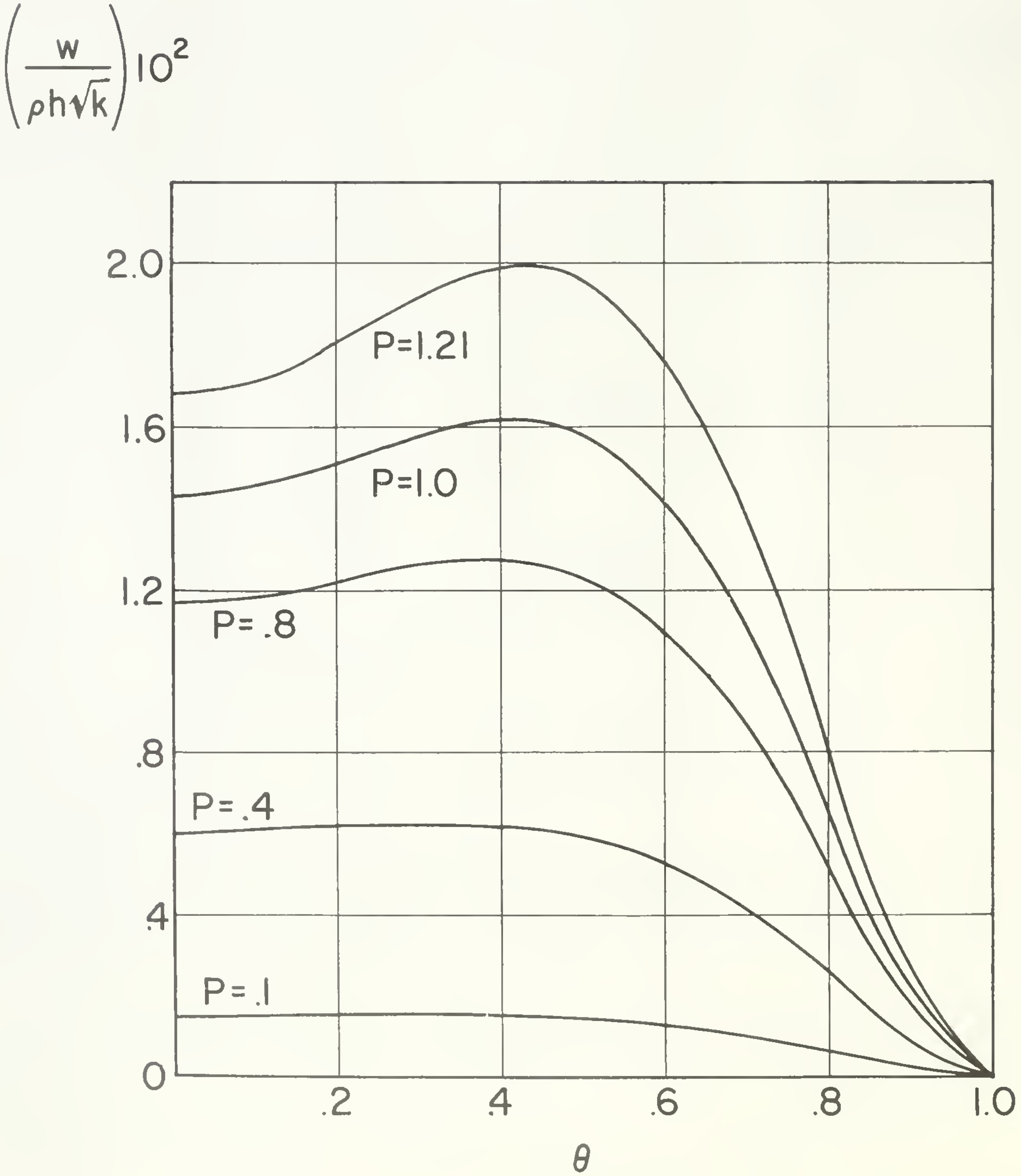

Fig. 7a

REDUCED LONGITUDINAL STRESS

$\rho = 32$ REGION II

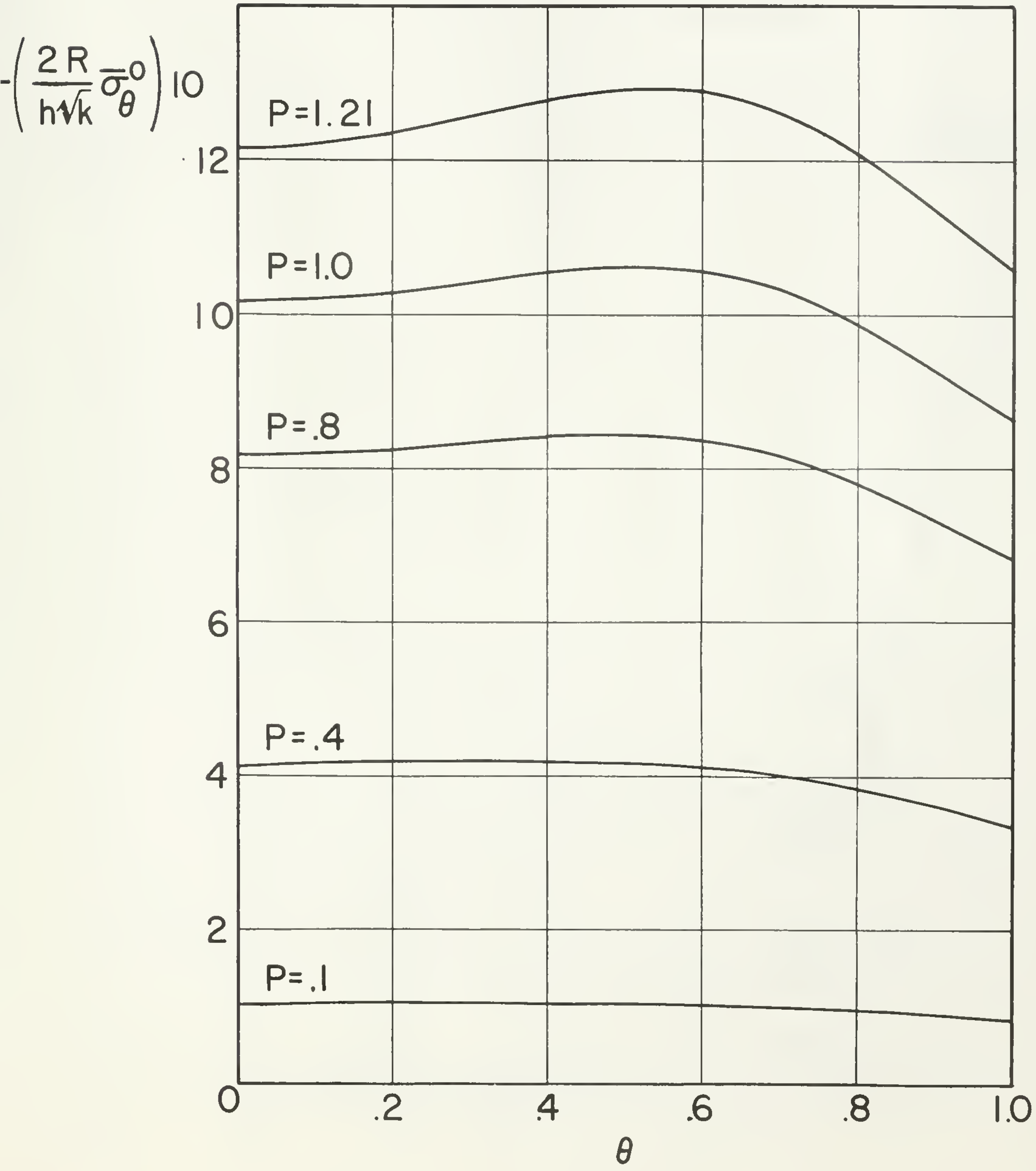

Fig. 7b

REDUCED LONGITUDINAL BENDING

STRESS—TOP SURFACE

$\rho = 32$ REGION II

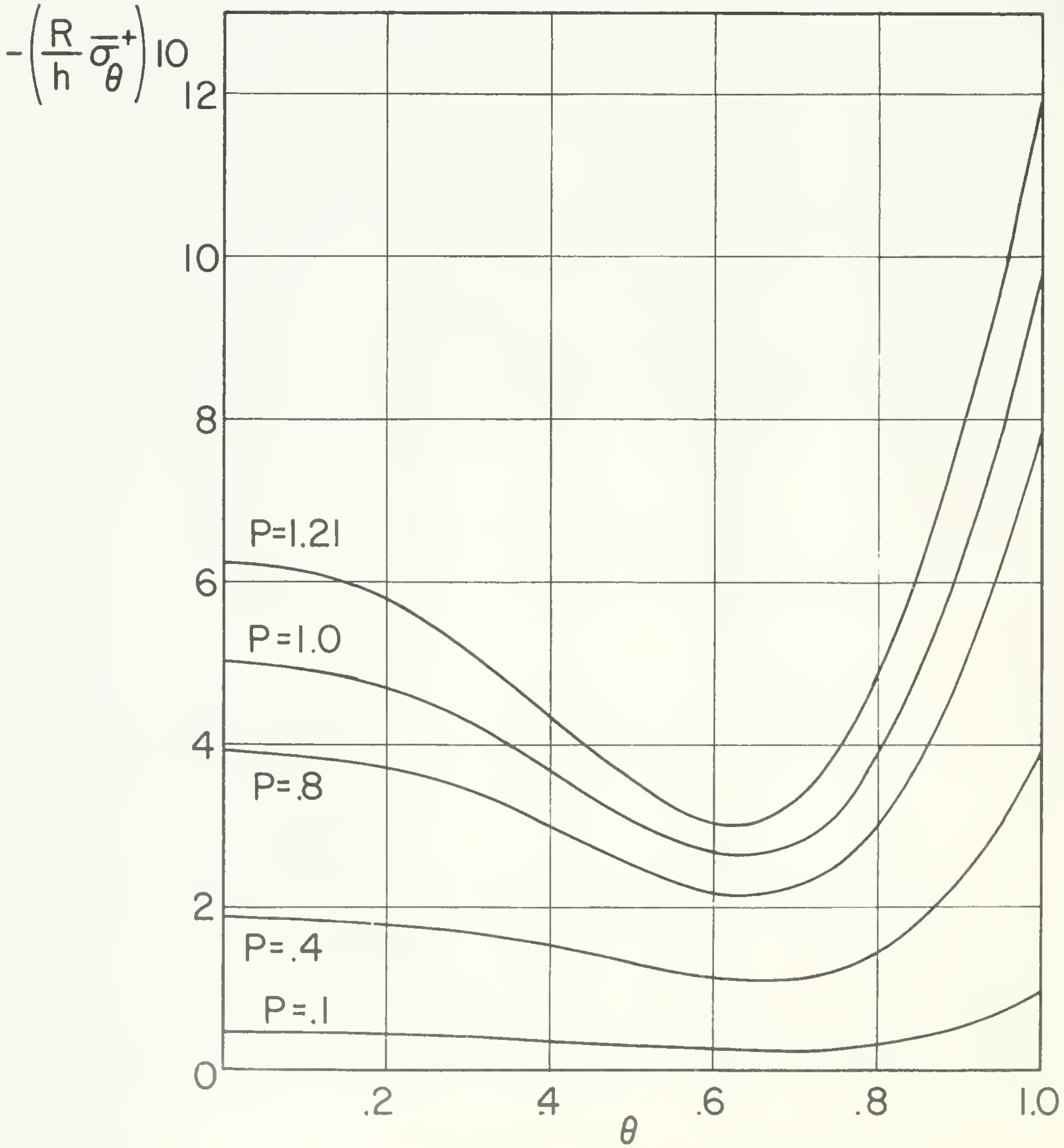

Fig. 7c

REDUCED LONGITUDINAL BENDING STRESS — BOTTOM SURFACE

$\rho = 32$ REGION II

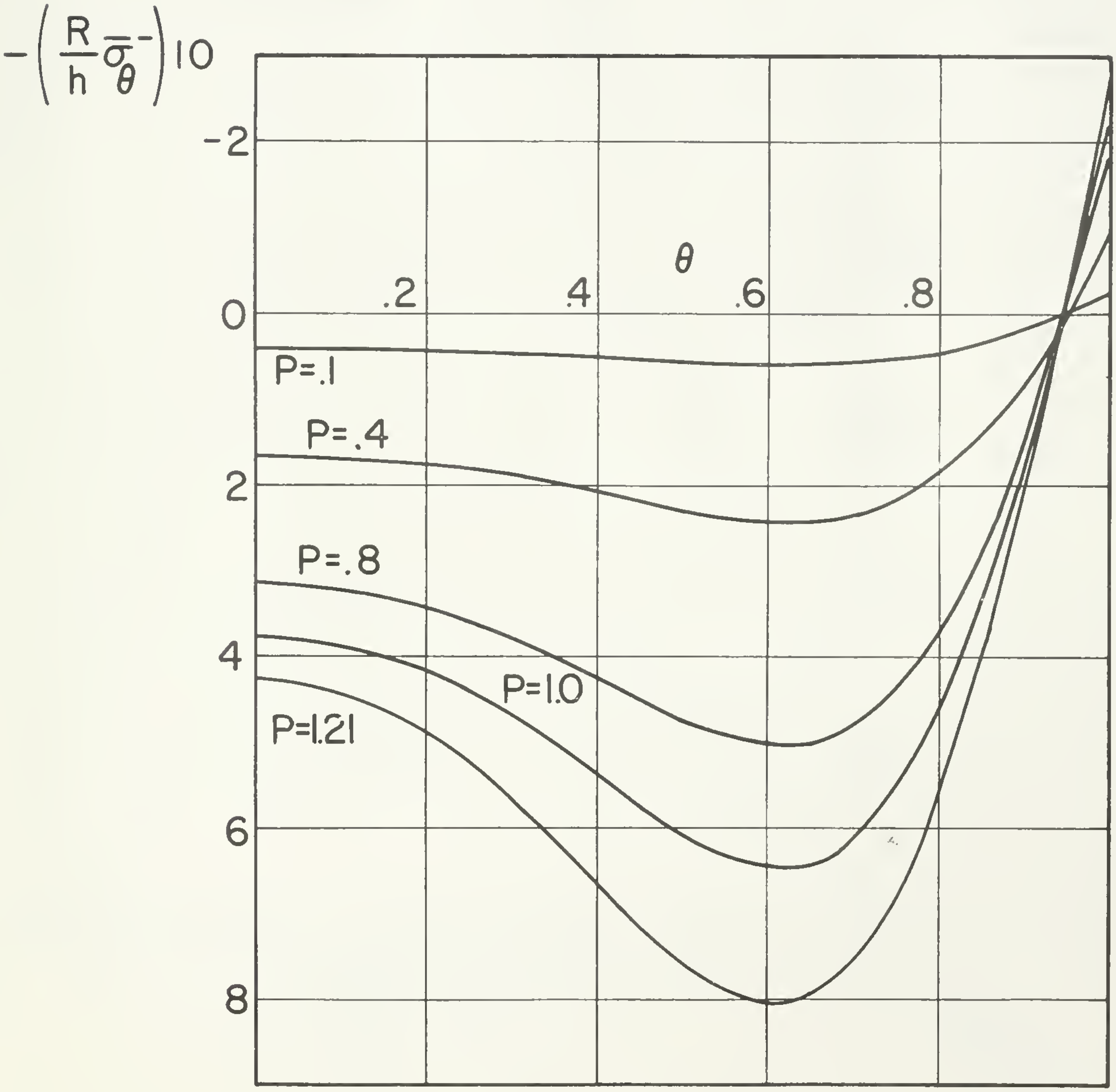

Fig. 7d

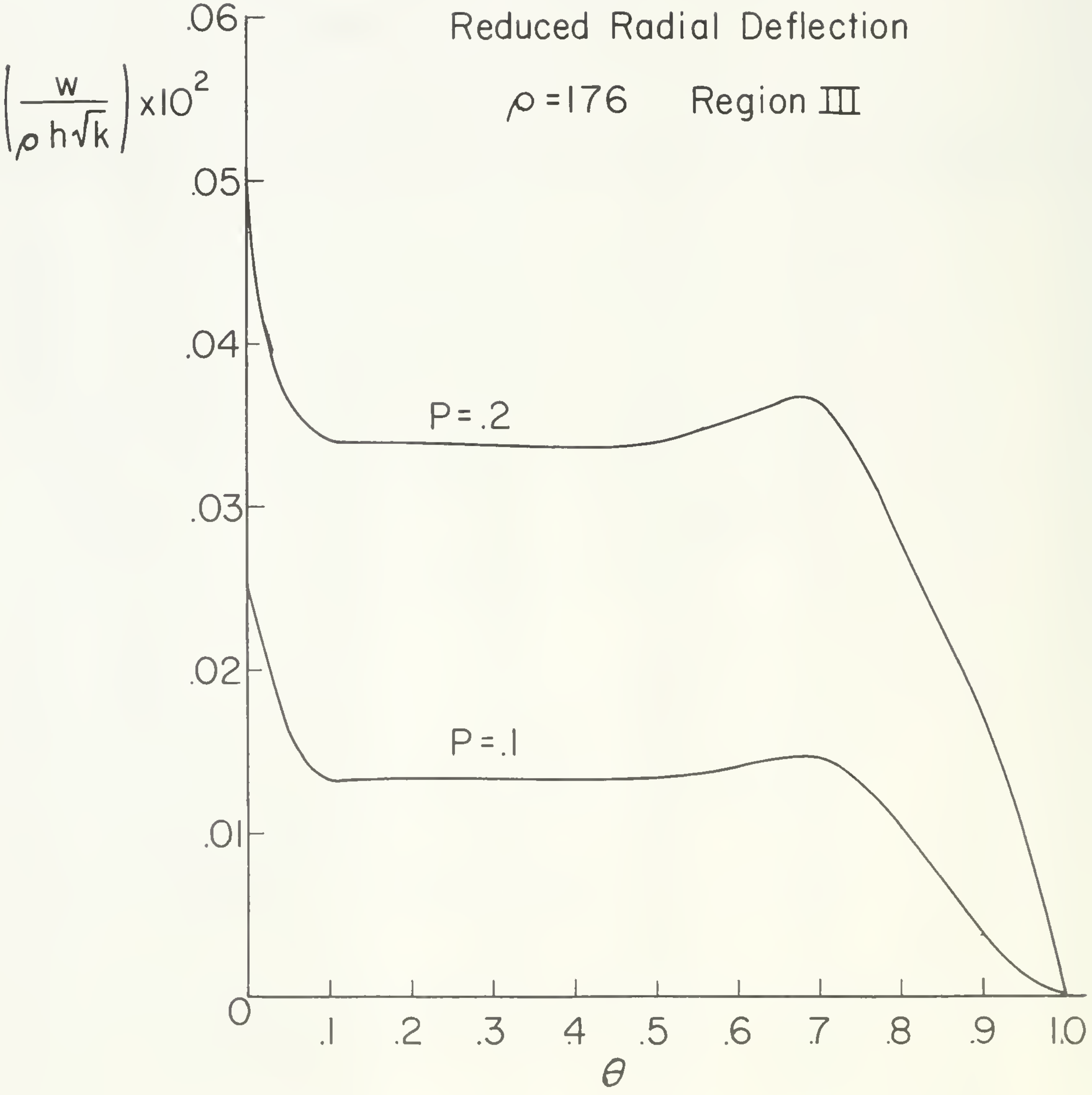
Reduced Radial Deflection
ρ = 176 Region III
$\left(\frac{w}{\rho h\sqrt{k}}\right) \times 10^2$
.06
.05
.04
.03
.02
.01
0
P = .2
P = .1
.1
.2
.3
.4
.5
.6
.7
.8
.9
1.0
θ

Fig. 8

REDUCED RADIAL DEFLECTION
AT P = 1.0

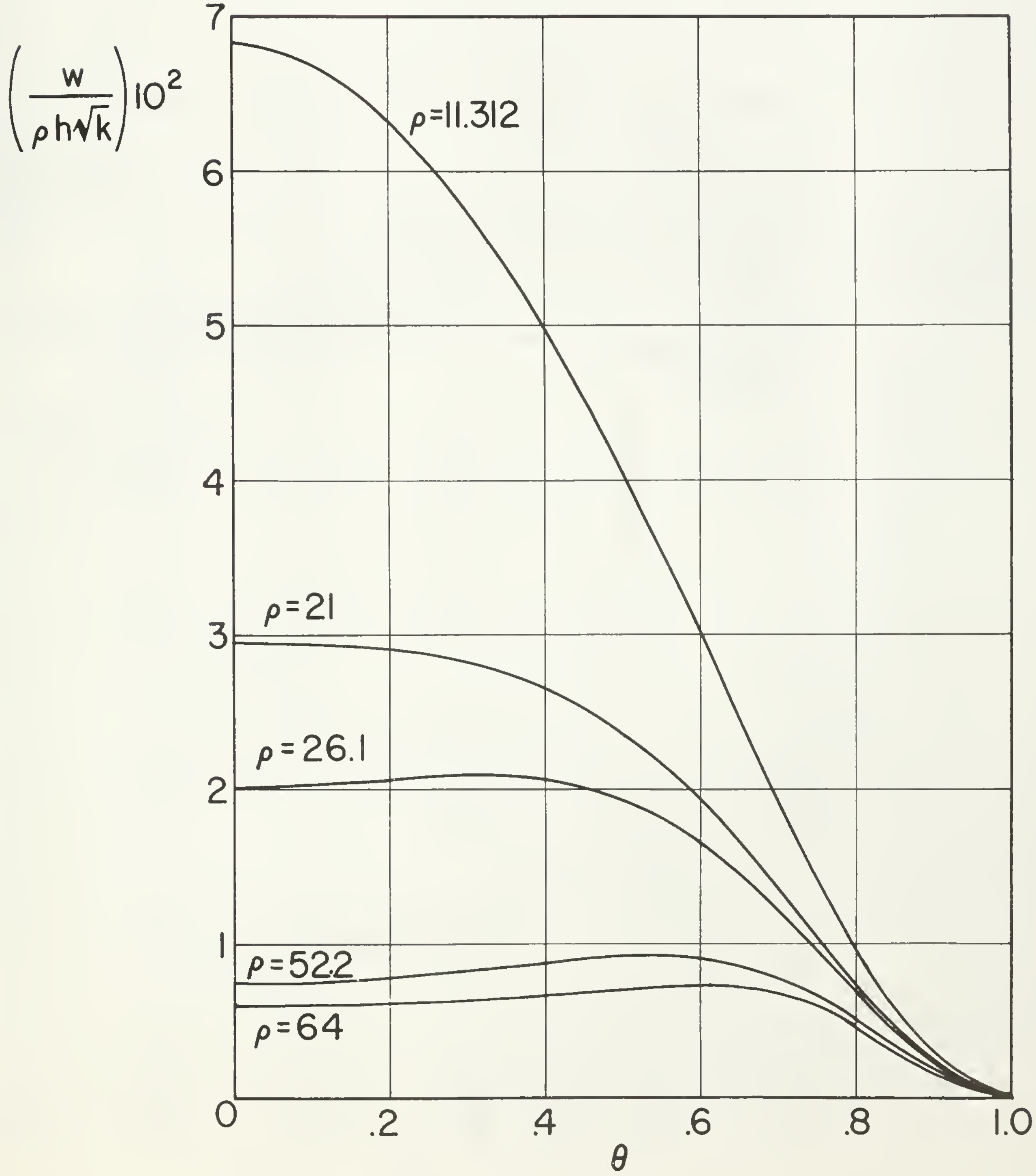

Fig. 9a

REDUCED LONGITUDINAL STRESS
AT P=1.0

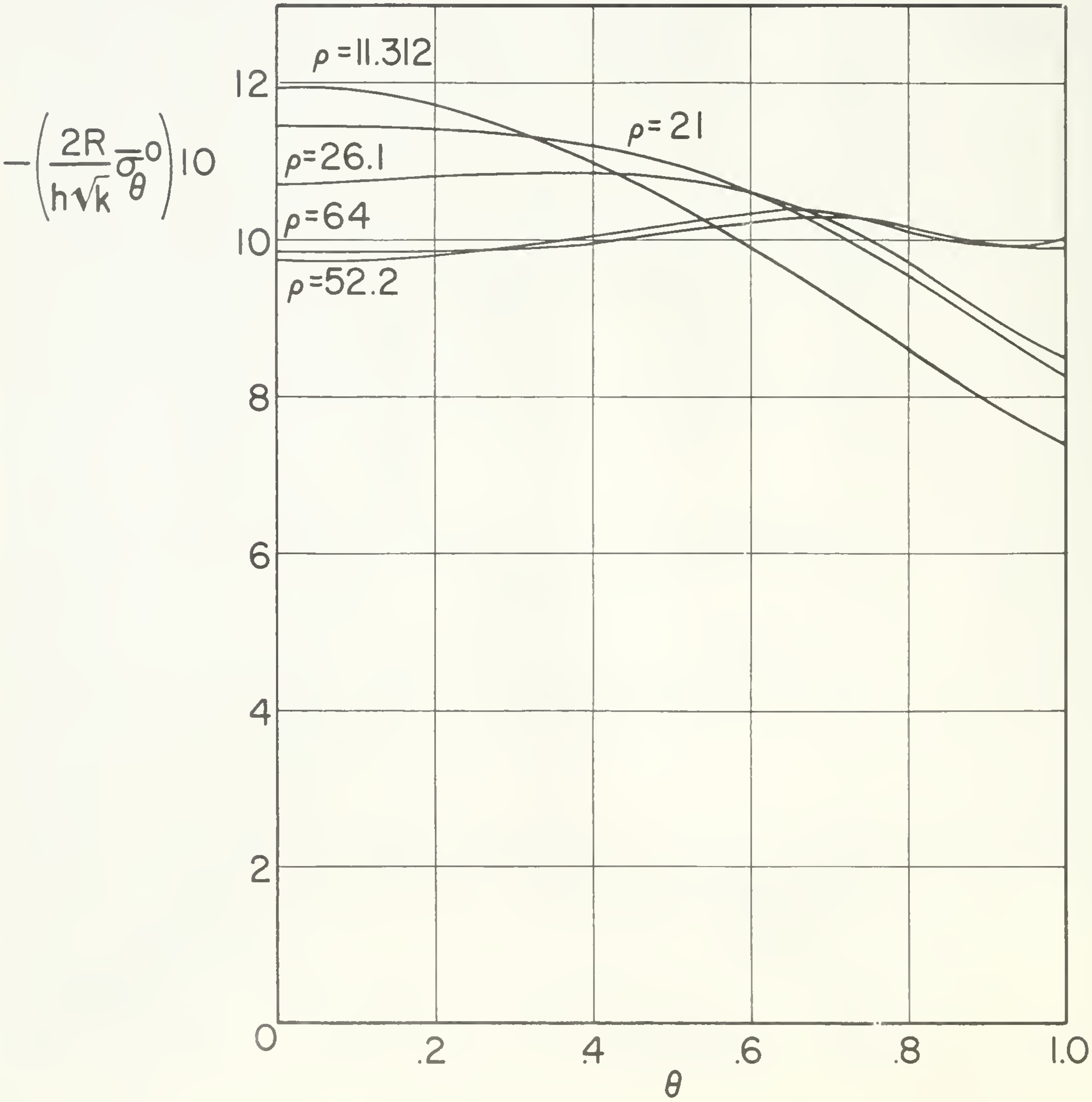

Fig. 9b

REDUCED LONGITUDINAL BENDING STRESS—TOP SURFACE AT P=1.0

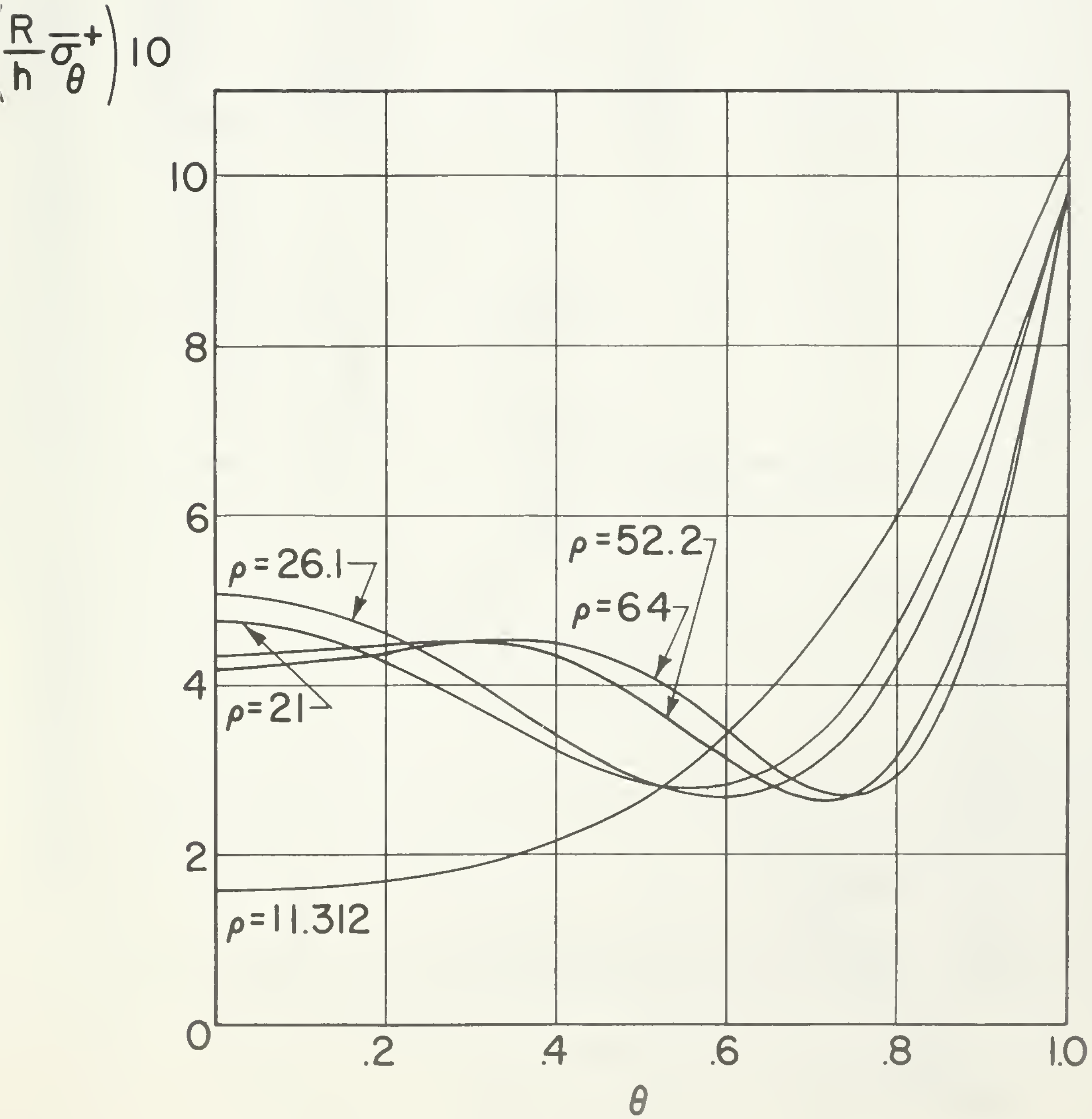

Fig. 9c

REDUCED LONGITUDINAL BENDING STRESS – BOTTOM SURFACE AT P=1.0

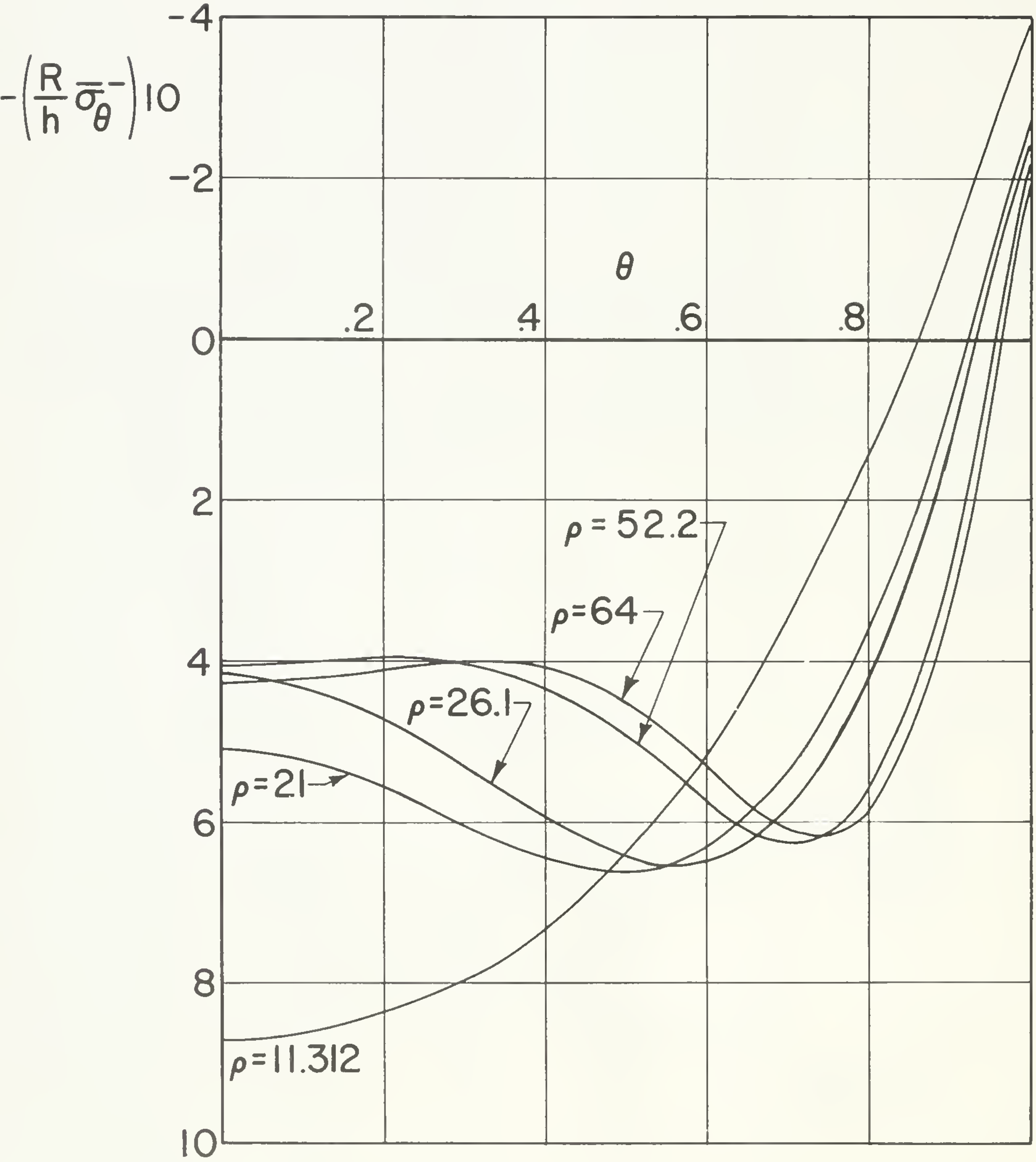

Fig. 9d

LOAD PARAMETER VS REDUCED DEFLECTION AT CENTER

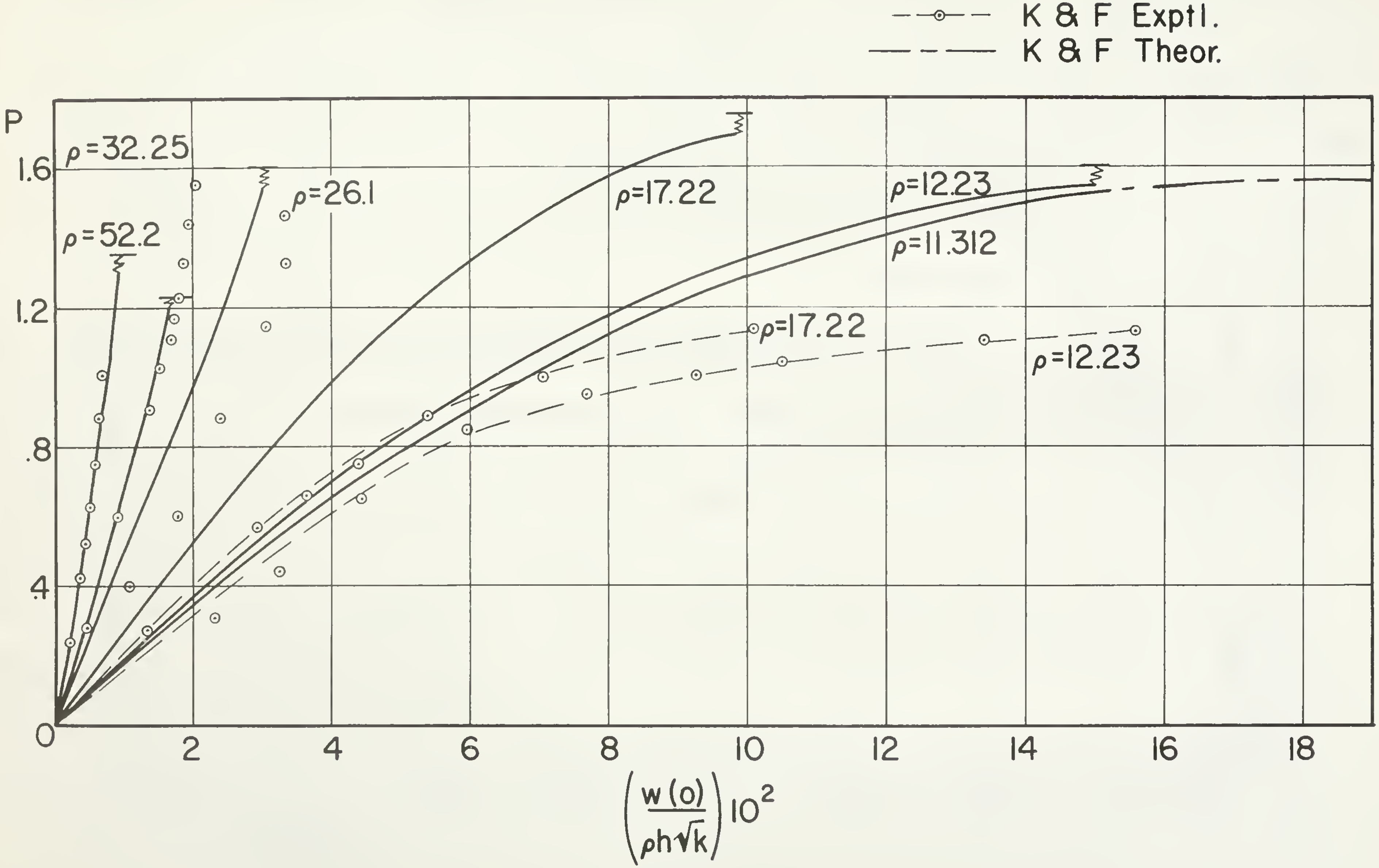

Fig. 10

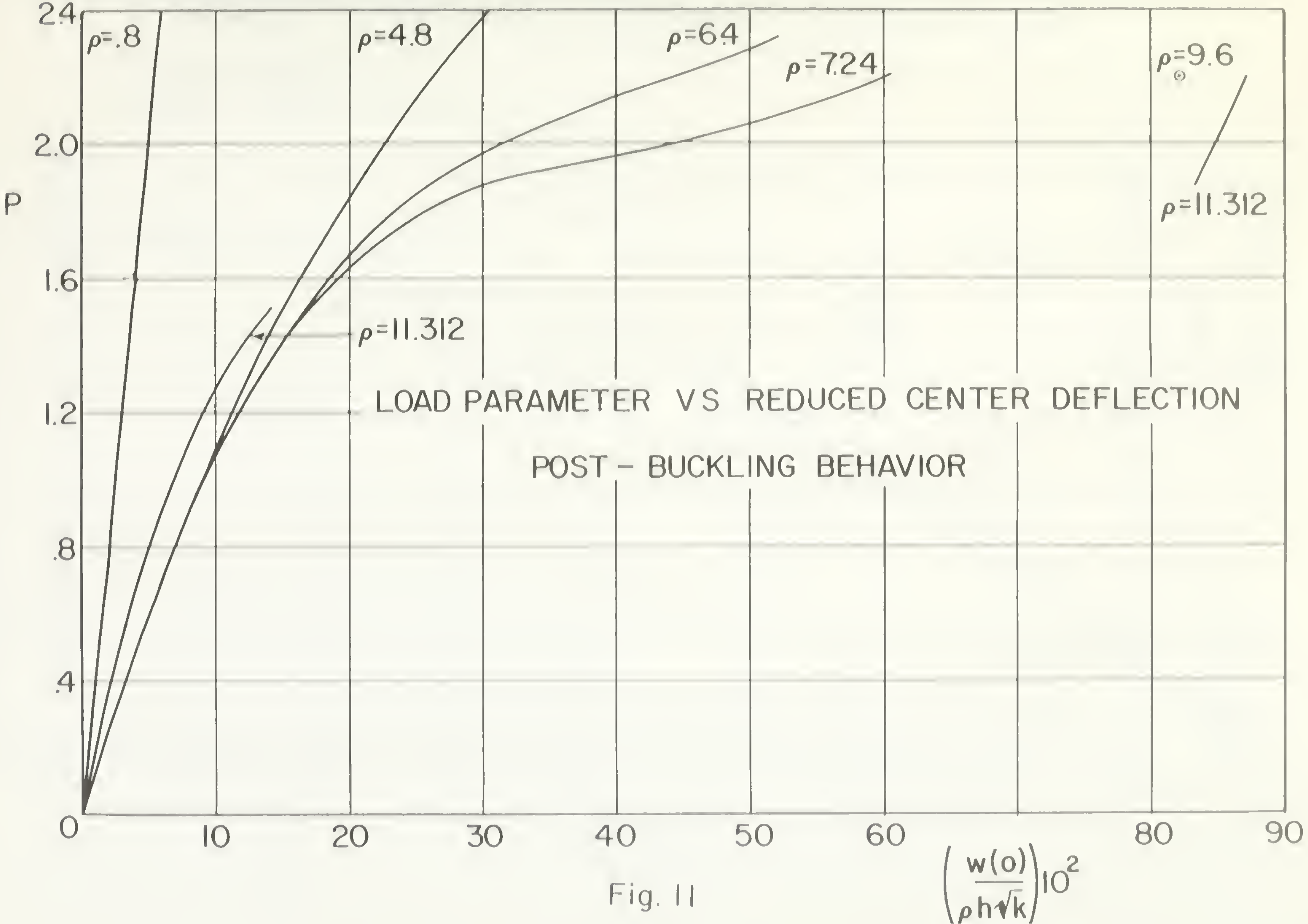
LOAD PARAMETER VS REDUCED CENTER DEFLECTION
POST - BUCKLING BEHAVIOR
P
2.4
2.0
1.6
1.2
.8
.4
0
10
20
30
40
50
60
80
90
$\left(\frac{w(o)}{\rho h\sqrt{k}}\right)10^2$
ρ=.8
ρ=4.8
ρ=6.4
ρ=7.24
ρ=9.6
ρ=11.312
ρ=11.312

Fig. 11

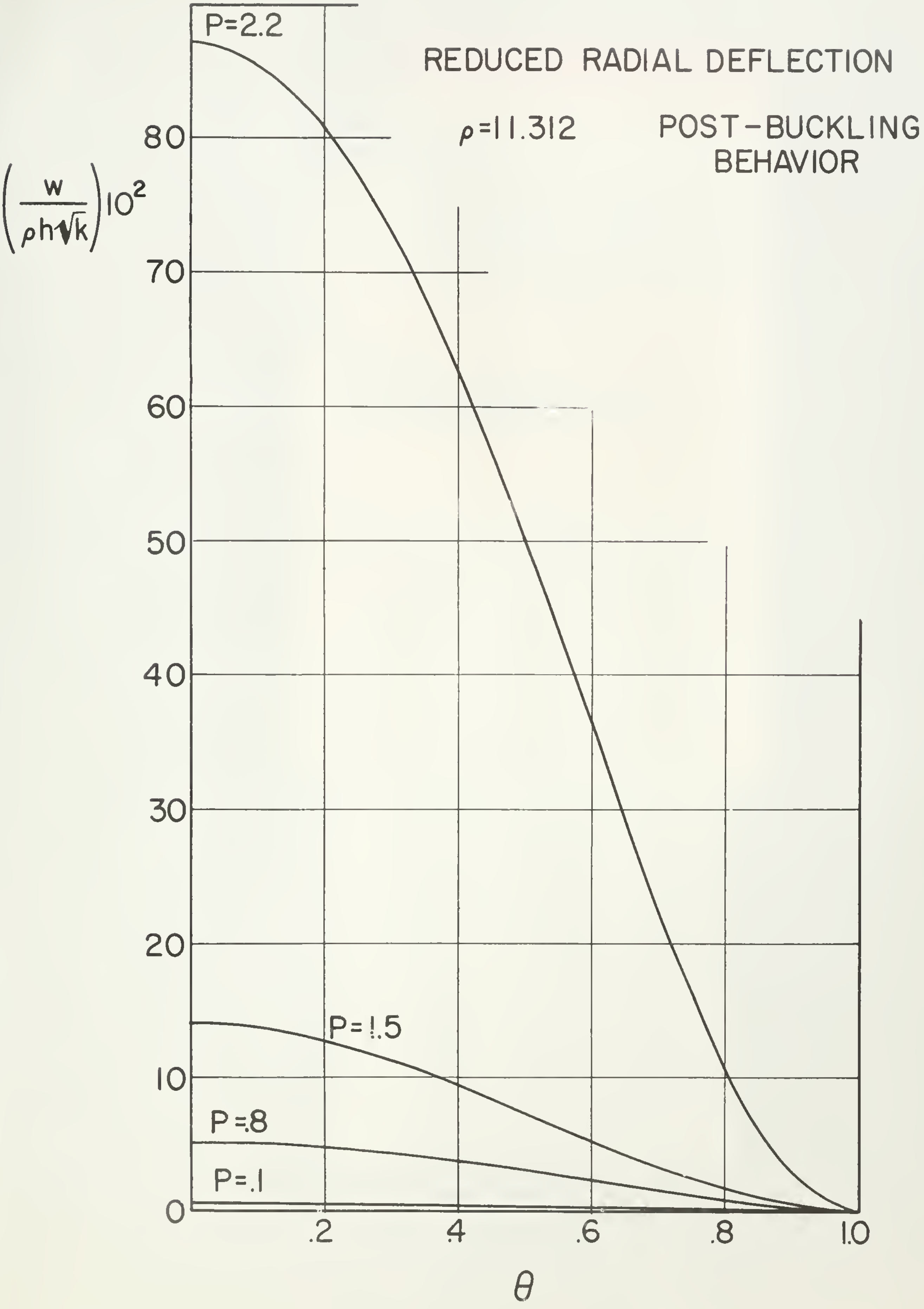
REDUCED RADIAL DEFLECTION
ρ=11.312
POST-BUCKLING BEHAVIOR
(w/ρh√k)10²
P=2.2
P=1.5
P=.8
P=.1
0
10
20
30
40
50
60
70
80
.2
.4
.6
.8
1.0
θ

Fig. 12

NYU
NYO-

NYU
NYO
7695 Reiss
AUTHOR

TITLE Non-linear deflections

of shallow spherical....

DATE DUE

NYU
NYO
7695
Reiss
Non-linear deflections of
shallow spherical....

Date Due

1 June 61			
NOV 1 1 86			
GB	PRINTED	IN U. S. A.	